

Carbon, iron and sulphur cycling in the sediments of a Mediterranean lagoon (Ghar El Melh, Tunisia)

Oueslati, Walid; van de Velde, Sebastiaan; Helali, M. Amine; Added, Ayed; Aleya, Lotfi; Meysman, Filip J.R.

DOI

[10.1016/j.ecss.2019.03.008](https://doi.org/10.1016/j.ecss.2019.03.008)

Publication date

2019

Document Version

Accepted author manuscript

Published in

Estuarine, Coastal and Shelf Science

Citation (APA)

Oueslati, W., van de Velde, S., Helali, M. A., Added, A., Aleya, L., & Meysman, F. J. R. (2019). Carbon, iron and sulphur cycling in the sediments of a Mediterranean lagoon (Ghar El Melh, Tunisia). *Estuarine, Coastal and Shelf Science*, 221, 156-169. <https://doi.org/10.1016/j.ecss.2019.03.008>

Important note

To cite this publication, please use the final published version (if applicable).
Please check the document version above.

Copyright

Other than for strictly personal use, it is not permitted to download, forward or distribute the text or part of it, without the consent of the author(s) and/or copyright holder(s), unless the work is under an open content license such as Creative Commons.

Takedown policy

Please contact us and provide details if you believe this document breaches copyrights.
We will remove access to the work immediately and investigate your claim.

Carbon, iron and sulphur cycling in the sediments of a Mediterranean lagoon (Ghar El Melh, Tunisia)

Walid Oueslati ^{1#}, Sebastiaan van de Velde ^{2,3}, M. Amine Helali ¹, Ayed Added ¹, Lotfi Aleya ⁴, Filip J. R. Meysman ^{3,5}

¹ Laboratoire des Ressources Minérales et Environnement, Département de Géologie, Faculté des Sciences de Tunis, Université de Tunis El Manar. 2092 Tunisie

² Department of Earth Sciences, University of California, Riverside, CA 92521, USA

³ Ecosystem Management Research Group, Department of Biology, University of Antwerp, Universiteitsplein 1, BE- 2610 Wilrijk (Antwerp), Belgium

⁴ Université de Bourgogne Franche-Comté, Laboratoire de Chrono-Environnement, UMR CNRS 6249, La Bouloie, F-25030 Besançon Cedex, France

⁵ Department of Biotechnology, Delft University of Technology, Van der Maasweg 9, 2629 HZ Delft, The Netherlands

Corresponding author: w.oueslati@gmail.com (Tel. +21623408116)

Published in: Estuarine & Coastal Shelf Sciences

Keywords: marine sediments, early diagenesis, pyrite formation, authigenic carbonate formation

Version: post-print (= peer-reviewed version, without publisher's layout)

Word count: Abstract: 296 / Text: 10805

ABSTRACT

Coastal lagoon sediments are important for the biogeochemical carbon cycle at the land-ocean transition, as they form hotspots for organic carbon burial, as well as potential sites for authigenic carbonate formation. Here, we employ an early diagenetic model to quantify the coupled redox cycling of carbon, iron and sulphur in the sediments of the shallow Ghar El Melh (GEM) lagoon (Tunisia). The model simulated depth profiles show a good correspondence with available pore water data (dissolved inorganic carbon, NH_4^+ , total alkalinity, Ca^{2+} , Fe^{2+} and SO_4^{2-}) and solid phase data (organic matter, pyrite, calcium carbonate and iron (oxyhydr)oxides). This indicates that the model is able to capture the dominant processes influencing the sedimentary biogeochemical cycling. Our results show that sediment of the GEM lagoon is an efficient reactor for organic matter breakdown (burial efficiency < 10 %), with an important role for aerobic respiration (32 %) and sulphate reduction (61 %). Despite high rates of sulphate reduction, free sulphide does not accumulate in the pore water, due to a large terrestrial input of reactive iron oxides and the efficient sequestration of free sulphide into iron sulphide phases. High pyrite burial ($2.2 \text{ mmol FeS}_2 \text{ m}^{-2} \text{ d}^{-1}$) prevents the reoxidation of reduced sulphide, thus resulting in a low total oxygen uptake ($4.7 \text{ mmol m}^{-2} \text{ d}^{-1}$) of the sediment and a relatively high oxygen penetration depth. The formation of pyrite also generates high amounts of alkalinity in the pore water, which stimulates authigenic carbonate precipitation ($2.7 \text{ mmol m}^{-2} \text{ d}^{-1}$) and leads to alkalinity release to the overlying water ($3.4 \text{ mmol m}^{-2} \text{ d}^{-1}$). Model simulations with and without an N-cycle reveal a limited influence of nitrification and denitrification on the overall organic matter diagenesis. Overall, our study highlights the potential role of coastal lagoons for the global carbon and sulphur cycle, and their possible contribution to shelf alkalinity, which increases the buffering capacity of the coastal ocean for CO_2 uptake.

INTRODUCTION

Coastal lagoons are shallow water bodies, oriented in parallel to the shoreline and separated from the ocean by a barrier that allows water exchange through one or more inlets. Bordering 13% of the world's present-day coast line, they are a common type of coastal ecosystems, typically resulting from the submergence of coastal plains during Holocene sea-level rise (Nichols and Allen 1981). Coastal lagoons are highly dynamic environments in terms of biogeochemistry, and they play an important role in the transport, modification and accumulation of organic matter at the land-ocean interface. Because of their proximity to land, lagoons receive considerable quantities of nutrients, which stimulates *in situ* primary production by microphytobenthos, macroalgae, and seagrasses (Bianchi 2007). At the same time, these lagoons receive considerable amounts of allochthonous carbon from terrestrial sources. Part of the locally produced as well as the imported organic carbon is stored in the sediments, making these coastal lagoons prime locations for marine organic matter burial (Burdige 2007) and rendering them an important "blue carbon" sink (McLeod et al., 2011).

In these shallow environments, the sediment plays an essential role in the biogeochemical cycling, as there is a close coupling with water column processes. Due to the high organic matter (OM) loading, sedimentary mineralisation rates are high, and oxygen is rapidly depleted in the first few millimetres of the sediment (Glud 2008). This favours the prevalence of anaerobic pathways of organic matter mineralisation, such as dissimilatory iron reduction and sulphate reduction. The biogeochemical cycles of sulphur and iron in the sediment are strongly intertwined, as ferrous iron and reduced sulphide readily precipitate as iron sulphide minerals, such as mackinawite, greigite and pyrite (Morse et al. 1987, Rickard and Morse 2005). The formation and burial of iron sulphides forms a source of alkalinity to the pore water in shallow marine environments (Stumm and Morgan 1996).

Recent studies have pointed out that the alkalinity generation in coastal sediments may increase the capacity of the coastal ocean to act as a potential sink for atmospheric CO₂ (Thomas et al. 2009; Faber et al. 2012; Brenner et al. 2016). Sedimentary alkalinity production can offset the effect of dissolved inorganic carbon production by respiration on the acidification of coastal waters, thus enhancing the uptake of atmospheric CO₂ (Hu and Cai 2011; Brenner et al. 2016). For example, in the North Sea, it has been estimated that as much as one-quarter of the overall CO₂ uptake may be driven by

alkalinity production in the intertidal flats of the southern North Sea (Thomas et al. 2009). This observation has recently sparked great interest in quantifying the rates and mechanisms of alkalinity production in coastal sediments (Cyronak et al. 2013; Faber et al. 2012; Rao et al. 2014; Rao et al. 2016; Brenner et al. 2016).

However, mechanisms that produce alkalinity in coastal sediments remain poorly understood (Rassmann et al. 2016), due to the complexity and competition of multiple reactions in anoxic sediments (Froelich et al. 1979; Van Cappellen and Wang 1996). The aim of the present study is to establish a quantitative understanding of biogeochemical cycling and alkalinity generation in the sediments of a Mediterranean lagoon. To address the objective, we compiled a dataset on pore water and solid phase geochemistry and analysed this dataset by means of reactive transport modelling. This model-data comparison enables a detailed insight into the coupled cycling of carbon, iron and sulphur, and allows to arrive at quantitative rate estimates for pyrite formation and authigenic carbonate formation, and the associated sedimentary alkalinity production or consumption in the lagoon.

1. MODEL FORMULATION

1.1 Site description

In Tunisia, lagoon environments cover a total area of 1100 km², and are distributed over the entire Mediterranean coastline from north to south (Moussa et al. 2005). These lagoons are of great ecological and economic importance, but are experiencing increasing anthropogenic pressure, being exposed to various types of environmental degradation resulting from agricultural, industrial and touristic activities (Oueslati et al. 2010; Zaaboub et al. 2015). The Ghar El Melh (GEM) is a shallow coastal lagoon in northern Tunisia, which is separated by a narrow vegetated sand strip from the Mediterranean Sea (Fig. 1). The lagoon has a total area of 35.6 km² and consists of three main parts (Ayache et al. 2009): the main lagoon where the field site of this study is located (26.7 km²), the smaller basin of Sebkheth El Ouafi in the southeast (5.2 km²) which is permanently connected to the main lagoon, and the small sub-lagoon of Sebkheth Sidi Ali El Mekki in the northeast (3.7 km²) that is isolated by embankments. The main lagoon is generally very shallow (average water depth = 0.8 m; maximum depth = 3.8 m), and therefore, the water column of the lagoon remains well homogenised throughout the year due to wind-induced mixing. A narrow channel

enables a restricted water exchange with the open sea (water residence time in the lagoon: 35 days; Rasmussen et al., 2009). The salinity shows strong seasonal variation, resulting from freshwater runoff in winter (lowest salinity ~32) and strong evaporation in summer (highest salinity ~49).

Five thousand years ago, the GEM lagoon was a large bay, open to the Mediterranean Sea, into which the Mejerda River discharged. Since then, the bay has been gradually filled up with fluvial sediment from the Mejerda River, thus evolving into the present day lagoon (Pimienta 1959; Paskoff 1981; Added et al. 2003). At the end of the nineteenth century, the Mejerda River drastically changed its course during a major flood, shifting its natural outlet to the south of the lagoon (Ayache et al. 2009). Subsequently, the river system became the subject of several human interventions. In 1939, the lower part of Mejerda River was embanked, which facilitated drainage to the Mediterranean and reduced overflow during floods, thereby reducing the sediment transport to the lagoon. In 1948, a diverting canal was constructed further south of the GEM lagoon, designed to evacuate excess flood flow, and this artificial waterway constitutes the current outlet of the Mejerda River (Paskoff 1994). Construction of dams in the catchment between 1950 and 1981 have further reduced the sediment transport to the Mediterranean (Zahar et al. 2008). At present, sediment is mainly supplied to the lagoon by flash floods and surface runoff from the small catchment. Likely there is also a net import of sediment from the Mediterranean, due to relatively high suspended matter concentrations in the coastal waters outside of the lagoon (Rasmussen et al. 2009).

While the sediment loading has decreased, the nutrient loading to the lagoon has increased over the last decades, due to intensification of agriculture in the catchment and the development of an industrial area to the west of the lagoon. Moreover, the lagoon receives untreated sewage from two towns and a catchment area of 131 km² (Ayache et al. 2009). As a consequence, the lagoon has shown signs of increasing eutrophication, such as an increasing cover of macroalgae (mainly *Cladophora*), and a decrease in the vegetation of seagrasses (Shili et al. 2002). Concentrations of chlorophyll-a in the water column vary between 2.2 mg m⁻³ in winter to 54 mg m⁻³ in summer (Moussa et al. 2005). The estimated net primary production is 104 g C m⁻² yr⁻¹ or 3,731 tonnes C year⁻¹ over the whole lagoon (Rasmussen et al. 2009). Benthic fauna (mostly annelids) are observed only in low abundances, so sediments are likely subject to low rates of bioturbation.

1.2 Sediment parameters

Fine cohesive surface sediments characterize the central depositional zone of the GEM lagoon, where the sampling site is located (N 37.132607° and E 10.190882°). Seagrasses (*Ruppia* sp., Dhib et al. 2013) and macroalgae are restricted to the shallower parts of the lagoon, and are not growing near the field site location, which was unvegetated. Coarse sieving of sediment reveals fragmented mollusc shells that strongly contribute to the carbonate fraction, as well as seagrass detritus that is transported from shallower parts of the lagoon and contributes to the organic matter pool (Rasmussen et al. 2009). We estimated sediment parameters from a variety of literature sources. A porosity depth profile was obtained from a 120 cm deep sediment core in the middle of the lagoon (Rasmussen et al. 2009; Fig. 2a). We fitted an exponentially decreasing depth relation $\phi_F(x) = \phi_F^\infty + (\phi_F^0 - \phi_F^\infty)\exp(-x/x_a)$ to this profile using non-linear regression (using the Gauss-Newton algorithm of the nls function from the R package CRAN:stats, R-version 3.4.0). This provided a surface porosity $\phi_F^0 = 0.83$, an asymptotic porosity at depth $\phi_F^\infty = 0.69$, and a characteristic attenuation depth $x_a = 19$ cm (Fig. 2a). Rasmussen et al. (2009) furthermore estimated the current sediment load as 42,200 tonnes per year (mean over the period 2003-2004), which provides an average sediment accretion velocity of 1.9 mm yr⁻¹ over the whole lagoon (assuming a porosity at depth $\phi_F^\infty = 0.69$ and a solid phase density $\rho_s = 2.66$ g cm⁻³). However, sediment accumulation is strongly spatially variable, and the deeper part in the central lagoon (where the field site is located) experiences the highest rate of sediment deposition. Sediment cores within this central part were retrieved in 2003 and dated using natural (²¹⁰Pb) and artificial (¹³⁷Cs) radionuclides (Rasmussen et al. 2009). The resulting ¹³⁷Cs profile showed a well-resolved peak at 20.5 cm that most probably records the 1963 fallout maximum from the atmospheric testing of nuclear weapons (Sanchez-Cabeza and Ruiz-Fernandez, 2012) (Fig. 2b). The sharp peak in the ¹³⁷Cs profile also indicates that the bioturbation intensity at the field site must be low, thus inducing little peak broadening. Overall, the core dating results suggest a fairly uniform mean sediment accumulation rate $F_{sed} = 0.226$ g cm⁻² yr⁻¹ over the period 1963-2003 (Flower et al. 2009), resulting in a mean sediment accretion velocity $v_s^\infty = F_{sed} / (\rho_s (1 - \phi_F^\infty)) = 2.8$ mm yr⁻¹ in the central part of the lagoon.

1.3 Solid phase and pore water dataset

The simulation output of a reactive transport model was compared to available depth profile data of pore water solutes and solid phase concentrations. This pore water dataset was assembled from a variety of previously reported field campaigns. Depth profiles of organic matter, pyrite (FeS_2), pH, particulate inorganic carbon (CaCO_3), dissolved iron (Fe^{2+}) and iron (hydr)oxides (FeOOH) were obtained from Oueslati (2011). Data on pore water sulphate (SO_4^{2-}), Dissolved Inorganic Carbon (DIC), ammonium (NH_4^+), total alkalinity (A_T) and dissolved calcium (Ca^{2+}) were obtained from Added (2001) and Added (2002). The details of the chemical analysis are also given in these references. Chromium reducible sulphur (CRS) was determined on dry sediments according to the Cr-reduction method of Canfield et al. (1986). Acid-volatile sulphide (AVS) was extracted from wet sediment using a hot-acid purge-and-trap technique (Berner, 1974). Reactive iron was extracted from dry sediment with cold 1M HCl (extraction time = 16h) following the method of Huerta-Diaz and Morse (1990). The pore water data were collected from the same location at two different times (1990 and 2006). Our primary objective was to make optimal use of the available data, and to investigate what can be learned about geochemical cycling in the GEM lagoon from this dataset. There are no indications that the Ghar El Melh lagoon has experienced drastic environmental changes in the last two decades, and so we do not expect a strong signature of transient diagenesis in the pore water. Furthermore, the sediment domain that is investigated (~70 cm sediment column) encompasses a period of about 150 years, which is a large time interval compared to the time between the two sampling events.

1.4 Reactive transport model

The aim of the biogeochemical model is to simulate the depth profiles of the main pore water and solid phase constituents in the sediment of the GEM lagoon. The biogeochemical model comprises a conventional early diagenetic model, which is the standard approach to describe reactive transport in marine sediments (Boudreau 1997; Meysman et al. 2003; Berg et al. 2003). The core of this reactive transport model consists of a set of mass balance equations of the advection-diffusion-reaction form (Boudreau 1997; Meysman et al. 2005). Adopting the assumption of steady-state compaction, the balance equation for a pore water solute becomes (Meysman et al. 2005):

$$\phi_F \frac{\partial C_i}{\partial t} = \frac{\partial}{\partial x} \left[\phi_F D_i \frac{\partial C_i}{\partial x} - \phi_F v_F C_i \right] + \alpha (C_i^{OW} - C_i) + \sum_k \gamma_{i,k} R_k \quad [1]$$

The quantity C_i represents the concentration of a dissolved compound in the pore water, C_i^{OW} is the value in the overlying water, ϕ_F denotes the porosity (implemented via an exponentially decreasing depth relation as described above), D_i is the sedimentary diffusion coefficient, and v_F is the advective velocity of the pore fluid. The quantities R_k represent the rates of the biogeochemical reactions (as detailed in the next section), where $\gamma_{i,k}$ is the stoichiometric coefficient of the i -th species in the k -th reaction. The molecular diffusion coefficient D_i^{mol} is first calculated as a function of temperature and salinity using the R package CRAN:marelac (Soetaert et al. 2010) and corrected for tortuosity according to the modified Wiessberg relation of Boudreau (1996b), i.e., $D_i = D_i^{mol} / (1 - 2 \ln \phi_F)$. The quantity α is the bio-irrigation coefficient, which is set to zero here, as we assume that the impact of burrowing fauna on the solute transport is minimal.

For solid components, the general diagenetic equation has the form (Meysman et al. 2005):

$$\phi_S \frac{\partial C_j}{\partial t} = \frac{\partial}{\partial x} \left[\phi_S D_B \frac{\partial C_j}{\partial x} - \phi_S v_S C_j \right] + \sum_k \gamma_{j,k} R_k \quad [2]$$

The solid volume fraction is calculated from porosity ($\phi_S = 1 - \phi_F$). The concentration C_j of a solid compound is expressed per unit volume of solid sediment. The bio-diffusion coefficient is set to a low value ($D_B = 0.1 \text{ cm}^2 \text{ yr}^{-1}$ over the first 10 cm), reflecting a low level of solid phase mixing. As discussed above, the model adopts a constant sediment accumulation rate $F_{sed} = 0.226 \text{ g cm}^{-2} \text{ yr}^{-1}$, determined from core dating. Under the assumption of steady state compaction (Meysman et al., 2005), the advective velocity of the solids at infinite depth can be calculated as $v_S^\infty = F_{sed} / (\rho_s \phi_S^\infty)$, where ρ_s represents the solid phase density, and $\phi_S^\infty = 1 - \phi_F^\infty$ with ϕ_F^∞ the porosity at infinite depth. Furthermore, compaction ceases at infinite depth, and so the advective velocity of the pore fluid must be the same as that of the solid phase, i.e., $v_F^\infty = v_S^\infty$.

Subsequently, one can calculate the advective velocity of solutes and solids throughout the model domain as $v_F(x) = (\phi_F^\infty / \phi_F(x)) v_F^\infty$ and $v_S(x) = (\phi_S^\infty / \phi_S(x)) v_S^\infty$ respectively (Meysman et al., 2005).

For all pore water constituents, a fixed concentration was imposed as a boundary condition at the sediment-water interface. The concentration values were obtained from measured bottom water conditions at the field site (Table 1). For the solid phase compounds, a constant flux was imposed at the upper boundary. At the lower boundary of the model domain ($L = 72$ cm), a no gradient condition was imposed for all compounds (pore water and solid phase).

1.5 Reaction set

The reaction set included in the model is listed in Table 2. Our goal was to keep the reaction set as concise as possible, thus providing a parsimonious description of biogeochemical cycling in the sediments of the GEM lagoon. The associated kinetic rate expressions are listed in Table 3 and were adopted from existing models of sediment biogeochemistry (Boudreau 1996a; Van Cappellen and Wang 1996; Berg et al. 2003; Meysman et al. 2003). In total, six different reactions were included in the reaction set. Organic matter in the sediment is microbially degraded via three different pathways: (1) aerobic respiration, (2) dissimilatory iron reduction and (3) sulphate reduction (denitrification is only included as a sensitivity test, and is not part of the core model).

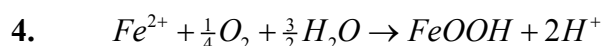
1. $CH_2O + O_2 \rightarrow HCO_3^- + H^+$
2. $CH_2O + 4FeOOH + 7H^+ \rightarrow HCO_3^- + 4Fe^{2+} + 6H_2O$
3. $CH_2O + \frac{4}{7}SO_4^{2-} + \frac{2}{7}Fe^{2+} \rightarrow HCO_3^- + \frac{2}{7}FeS_2 + \frac{3}{7}H^+ + \frac{2}{7}H_2O$

The mineralisation of organic matter (CH_2O) is described via classical kinetic expression, in which the mineralisation rate R_{min} linearly scales with the amount of organic matter that is present. Two types of organic matter are included (slow and fast decaying, as specified by a different mineralisation rate constant k). The release of

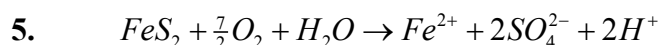
ammonium (NH_4^+) during mineralisation is specified by the ammonification rate $N_{\min} = (N/C) \cdot R_{\min}$, where (N/C) represents the nitrogen to carbon ratio of the organic matter. Both types of organic matter are assumed to have the same N/C ratio.

Iron reduction and sulphate reduction are suppressed under oxic conditions, which are implemented via a conventional limitation-inhibition formulation (Table 3; Soetaert et al. 1996). The degree of overlap between the zones iron and sulphate reduction is governed by the inhibition constant K_{FeOOH} . The ferrous iron (Fe^{2+}) released from reduction of iron hydroxides (FeOOH) accumulates in the pore water, and this way, it becomes subsequently available for pyrite formation (FeS_2). The pore water of the lagoon is found to be devoid of free sulphide (Added 2002), but sulphate reduction appears to be the dominant mineralisation pathway (Oueslati et al., 2010). Additionally, iron oxide reduction coupled to sulphide oxidation has previously been found to be of minor importance for the consumption of free sulphide, when compared to the precipitation of iron sulphide minerals (van de Velde and Meysman, 2016). Therefore, our model assumes a tight coupling between sulphate reduction and pyrite formation: all free sulphide generated by sulphate reduction is directly trapped as pyrite. This way the model formulation can be simplified, as no intermediate sulphur compounds (e.g. free sulphide H_2S , or elemental sulphur S^0) need to be included in the reaction set.

When ferrous iron is transported upward from deeper layers by diffusion, it is re-oxidised when it comes into contact with oxygen



In a similar fashion, pyrite is also re-oxidised in the oxic layer of the sediment



Both re-oxidation reactions are modelled via standard second order rate expressions (Table 3).

Dissimilatory iron reduction produces 8 moles of alkalinity per mole of carbon, while combined sulphate reduction / pyrite formation generates 0.57 moles of alkalinity per mole of carbon mineralised. Accordingly, anoxic mineralisation can release

substantial quantities of alkalinity to the pore water, which may increase the pH and promote the authigenic precipitation of carbonates.

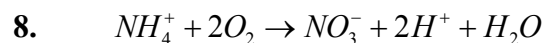


The carbonate precipitation rate was calculated according to the standard kinetic rate law, $R_{CP} = \phi_S k_{CP} (\Omega - 1)$, where the reaction rate scales with the saturation state of the pore water (Boudreau 1996a), and the reaction rate is zero for $\Omega \leq 1$ (no dissolution). The saturation state was calculated as $\Omega = [Ca^{2+}] a_2 \sum CO_2 / K_{SP}$ where the ionisation constant $a_2 = K_1 K_2 / ([H^+]^2 + K_1 [H^+] + K_1 K_2)$ represents the carbonate fraction of the dissolved inorganic carbon (Hofmann et al. 2010). The solubility product of calcite, K_{SP} , and the apparent equilibrium constants K_1 and K_2 of the carbonate system were calculated as a function of temperature and salinity using CRAN:AquaEnv, a dedicated R-package for acid-base and CO₂ system calculations (Hofmann et al. 2010). Specifically, for the carbonate equilibria, we used the relationships provided by Millero et al. (2006). The proton concentration $[H^+]$, or equally the $pH = -\log_{10}([H^+])$, was not included as state variable in the model. As protons are consumed or produced in nearly all biogeochemical reactions, and proton concentrations are low, the accurate model prediction pH depth profiles in sediments remains challenging. To avoid this complexity, we simply imposed the observed pH profile upon the model. To this end we fitted an exponential decreasing depth profile $pH(x) = pH_\infty + (pH_0 - pH_\infty) \exp(-x/x_{pH})$ to the available data (Fig. 3h; fitting parameters $pH_0 = 8.4$; $pH_\infty = 7.2$; $x_{pH} = 12$ cm).

The dataset does not include pore water nitrate, which makes it difficult to constrain the rates nitrification and denitrification. To still investigate the impact of the N cycling on pore water depth profiles and organic matter degradation, a sensitivity test was performed. To this end, the standard model was extended with denitrification.



and nitrification reactions



The associated kinetic rate expressions for these reactions are given in Table 3.

1.6 Numerical solution

Altogether, the model includes 11 state variables: the concentration of two types of organic matter [CH_2O_f] and [CH_2O_s], ammonium [NH_4^+], oxygen [O_2], sulphate [SO_4^{2-}], ferrous iron [Fe^{2+}], iron oxyhydroxide [$FeOOH$], pyrite [FeS_2], dissolved inorganic carbon (DIC, modelled as bicarbonate [HCO_3^-]), calcium [Ca^{2+}], calcium carbonate [$CaCO_3$]. In the sensitivity model run, nitrate [NO_3^-] was additionally included. We have chosen to not explicitly model the pH, but to externally impose the pH depth profile upon the model. Hence, the modelled bicarbonate concentration [HCO_3^-] actually represents DIC, and the speciation of the carbonate system is done at each depth based on the imposed pH (i.e. the calculation of the factor a_2 – see section 1.5). A numerical solution procedure for the resulting partial differential equations was implemented in the open-source programming language R, following the procedures of Hofmann et al. (2008) and Soetaert and Meysman (2012). Following the method-of-lines to solve diagenetic models (Boudreau et al., 1996a), we expanded the spatial derivatives of the partial differential equations over the sediment grid using finite differences, using the dedicated routines of the R-package CRAN:ReacTran (see Soetaert and Meysman 2012 for details). This finite difference grid was obtained by dividing the sediment domain (thickness $L = 72$ cm) into a non-uniform grid of 100 sediment layers (finer resolution near the sediment water interface). After finite differencing, the resulting set of ordinary differential equations was integrated using the stiff equation solver *vode* (Brown et al., 1989) as implemented in the R-package CRAN:deSolve (Soetaert et al. 2012). The steady state solution was calculated by running the model dynamically to steady state using the function *steady.1D* from the CRAN:rootSolve package (Soetaert and Herman 2009). The alkalinity is *a posteriori* calculated from the DIC and pH as $A_T = (a_1 + 2a_2)[HCO_3^-] - [H^+]$, where a_1 and a_2 are the ionisation constants of the carbonate system. This calculation neglects the contributions of the minor acid-base systems (borate, silicate, ammonium), as their contribution in pore waters is relatively small.

1.7 Model parameterisation

Table 1 provides an overview of all parameters, which are classified into three categories, depending on the way that parameters values were constrained. The first category, referred to as “Environmental parameters”, could be directly constrained based on the available field data (e.g. temperature, salinity, porosity depth profile, pH depth profile, composition of the overlying bottom water at the field site). The second category, denoted “Biogeochemical parameters”, includes parameters that also feature in conventional models of sediment geochemistry. This includes the parameters in the kinetic rate expressions of organic matter mineralisation and subsequent re-oxidation reactions, as well as the parameters describing the precipitation of calcium carbonate. The values of these biogeochemical parameters were constrained based on previous early diagenetic model studies (Table 1 provides the values and references).

2. RESULTS

2.1 Organic matter mineralisation

The sediments underlying the shallow warm waters of the GEM lagoon support a high organic matter mineralisation rate. The depth profile of organic carbon (OC) shows a decrease from 2.6% near the sediment water interface to 0.25% at 40 cm depth. The model closely reproduces the decrease of organic carbon with depth (Fig. 3a) and estimates the input of organic carbon to the sediment at $14.4 \text{ mmol C m}^{-2} \text{ d}^{-1}$, of which 91% is mineralised ($13.1 \text{ mmol C m}^{-2} \text{ d}^{-1}$) and only 9% is buried past the 70 cm depth horizon ($1.3 \text{ mmol C m}^{-2} \text{ d}^{-1}$).

The organic matter arriving at the sediment surface was assumed to belong to two classes with different reactivity. The model estimates that 55% of the organic matter is highly reactive (decay constant $k = 0.5 \text{ yr}^{-1}$), while the remainder is slowly decaying (45% with $k = 0.02 \text{ yr}^{-1}$). The calculation of the remineralisation length ($\lambda = v_{sed} / k$ where $v_{sed} = (\phi_s^\infty / \phi_s^0) v_s^\infty = 0.5 \text{ cm yr}^{-1}$ is the sedimentation velocity at the sediment-water interface and k is the decay constant) illustrates that the highly reactive fraction already disappears within the first centimetre of the sediment, while the slowly decaying fraction mineralises over a characteristic depth scale of ~ 25 centimetres. Hence, the disappearance of the highly reactive organic matter fraction is difficult to constrain with a cm-scale resolution of slicing of the sediment.

Oxygen depth profiles have not been recorded in the GEM lagoon, and so no data-model comparison can be made. The model predicts an oxygen penetration depth of 13 mm (operationally defined as the depth where $[O_2] < 1 \mu M$) (Fig. 3b). The total oxygen uptake (TOU) of the sediment is estimated by the model at $4.7 \text{ mmol m}^{-2} \text{ d}^{-1}$. This TOU is 2.8 times lower than the total mineralisation rate of organic matter ($13.1 \text{ mmol C m}^{-2} \text{ d}^{-1}$ as discussed above). In the absence of bio-irrigation by infauna, this large difference between the TOU and the carbon mineralisation rate indicates that a substantial amount of the reduced compounds formed during mineralisation are buried rather than re-oxidised with oxygen. In the model, the burial of pyrite ($2.3 \text{ mmol FeS}_2 \text{ m}^{-2} \text{ d}^{-1}$) acts the primary sink for reduced compounds (i.e., the main sink for electrons derived from organic matter oxidation) (Fig. 3d). Since 3.5 moles of O_2 are needed to fully oxidise one mole of pyrite; one would need $8.1 \text{ mmol O}_2 \text{ m}^{-2} \text{ d}^{-1}$ to fully re-oxidise the burial flux of pyrite. Thus, the discrepancy between the TOU and the organic carbon mineralisation rate is explained by the high burial flux of pyrite.

The pore water shows an accumulation of DIC and NH_4^+ over the first 30 centimetres, after which the end-products of OM mineralisation reach plateau concentration values (Fig. 3e,f). While DIC accumulates to relatively high values (10 mM at 30 cm depth), the NH_4^+ concentrations only amount to 230 μM . To obtain a good fit to both depth profiles (Fig. 3e,f), the model required a very high C/N ratio (C/N = 50) for both the fast and slowly decaying organic matter fractions. The simulated net effluxes from the sediment of DIC and NH_4^+ are $10.34 \text{ mmol C m}^{-2} \text{ d}^{-1}$ and $0.26 \text{ mmol N m}^{-2} \text{ d}^{-1}$ respectively. The difference between the DIC efflux from the sediment and the mineralisation rate is explained by carbonate precipitation ($2.68 \text{ mmol C m}^{-2} \text{ d}^{-1}$) that takes place at depth (Fig. 3i).

2.2 Iron and sulphur cycling

In the GEM lagoon sediment, sulphate shows a progressive decrease with depth from 28 mM at sediment-water interface to below 15 mM in deeper sediment horizons (Fig. 3c). Accordingly, organoclastic sulphate reduction is not able to completely exhaust the sulphate pool in the sediment. Still, sulphate reduction is the dominant pathway of organic matter mineralisation (61%) in the GEM sediment, while aerobic degradation accounts for 32% of the total carbon mineralisation and dissimilatory iron reduction is responsible for 7% (Fig. 4a). The simulated depth distribution of aerobic respiration dominates the top centimetre, while below this, the depth distributions of sulphate

reduction and dissimilatory iron reduction show a substantial degree of vertical overlap (Fig. 4b).

The simulated concentration depth profile of pore water Fe^{2+} shows a subsurface maximum and matches the data profile well (Fig. 3k). Ferrous iron increases from near-zero values at the sediment-water interface to a subsurface maximum (0.27 mM) at 7 cm depth, after which the concentration gradually decreases to reach < 0.01 mM at 70 cm depth. Although the shape of the depth profile is similar, the model simulation overpredicts the stock of reactive iron (oxyhydr)oxides in the sediment. The FeOOH profile sharply decreases within the first 5 centimetres, after which it more gradually declines with depth (Fig. 3l). The concentration profile of pyrite (FeS_2) forms almost a mirror image of the FeOOH profile (Fig. 3d), suggesting a stoichiometric conversion of FeOOH into FeS_2 . The FeS_2 increased from near-zero values near the surface to > 1 wt-% S by weight at depth. The simulated input flux of FeOOH to the sediment is $2.50 \text{ mmol Fe m}^{-2} \text{ d}^{-1}$, while the burial flux of pyrite amounts to $2.23 \text{ mmol Fe m}^{-2} \text{ d}^{-1}$, thus suggesting a conversion efficiency of > 0.89 of FeOOH into FeS_2 . Yet, as noted above, the FeOOH at depth appears to be overpredicted by the model, thus indicating that in reality, the conversion efficiency is likely even higher.

2.3 Carbonate dynamics

Alkalinity is assumed to be dominated by the carbonate system and so experimentally determined alkalinity values are compared to modelled HCO_3^- concentrations. As the pH is not explicitly modelled, but externally imposed, HCO_3^- concentrations actually represent DIC (and not the bicarbonate ion specifically). The measured alkalinity depth profile (A_T) shows a similar evolution as the DIC profile, and increases from 2 mM to 12 mM over the first 30 cm, while the pore water pH decreases from 8.1 near the sediment-water interface to 7.3 over the same depth range (Fig. 3h). The pore water Ca^{2+} concentration quickly decreases in the first 10 centimetres (from 18 to 12 mM) followed by a more gradual decrease with depth (to less than 5 mM at 70 cm). The sediment of the GEM lagoon is generally rich in carbonates (mean CaCO_3 content $\sim 40\%$ by weight). The CaCO_3 data showed a gradually increase with depth from 38.4 to 44.2 %, and together with the pore water Ca^{2+} decrease, this hence indicates substantial carbonate precipitation.

3. DISCUSSION

3.1 Organic matter budget

Organic matter is an important driver for the early diagenetic processes in the sediment and is either derived from the water column by sedimentation or locally produced by benthic primary production. Based on catchment nutrient budgets and ecosystem modelling (Rasmussen et al. 2009), the mean yearly net primary production within the GEM lagoon (from phytoplankton, macroalgae and seagrass) has been estimated at $117 \text{ g C m}^{-2} \text{ yr}^{-1}$ (or equally $26.7 \text{ mmol C m}^{-2} \text{ d}^{-1}$). Similarly, the anthropogenic input of organic carbon from land has been estimated at $8.2 \text{ mmol C m}^{-2} \text{ d}^{-1}$, while there is a small net export to the Mediterranean of $2.3 \text{ mmol C m}^{-2} \text{ d}^{-1}$. The sedimentary OM mineralisation rate as estimated for the GEM lagoon by the diagenetic model here ($13.1 \text{ mmol m}^{-2} \text{ d}^{-1}$) is comparable to rates reported by Dedieu et al. (2007) for the Thau lagoon (France), but lower than the value reported for the Fogliano lagoon in Italy (Hull et al. 2008). In general, the mineralisation rates reported for Mediterranean lagoons are lower than those of tropical lagoons (Table 4).

The sediment receives a total input of $14.4 \text{ mmol C m}^{-2} \text{ d}^{-1}$ of organic carbon, of which ($13.1 \text{ mmol C m}^{-2} \text{ d}^{-1}$) is mineralised, and $1.3 \text{ mmol C m}^{-2} \text{ d}^{-1}$ is ultimately buried. Combined with the carbon flows above, mass budgeting provides a heterotrophic water column respiration of $(26.7 + 8.2 - 2.3 - 14.4) = 18.2 \text{ mmol C m}^{-2} \text{ d}^{-1}$. Accordingly, 58% of the respiration takes place in the water column and 42% in the sediment, and so the sediment compartment emerges as an important site for mineralisation and nutrient recycling. However, it should be noted that the deeper part of the GEM lagoon functions as a depot centre (sedimentation velocity of 2.8 mm yr^{-1} as estimated by radionuclide dating versus an average sedimentation velocity of 1.9 mm yr^{-1}). Therefore, the contribution of the sedimentary component to the total respiration of the Ghar El Melh lagoon should be regarded as an upper bound.

In general, it is thought that shallow coastal ecosystems, like estuaries and lagoons, act as sinks for organic carbon (Nellemann et al. 2009; Smith et al. 2015; Watanabe and Kuwae 2015). This capacity to sequester OC is driven both by the anoxic state of pore waters (favouring preservation) as well as the high input of organic matter, either allochthonous (high terrestrial carbon input due proximity to land; Regnier et al. 2013) or autochthonous (high local primary production rate due to riverine nutrient input; Bianchi 2007). In general, the sedimentation rate is considered a crucial factor governing the OC burial efficiency (Canfield, 1994). At high sedimentation rates ($> 0.1 \text{ g cm}^{-2} \text{ yr}^{-1}$), 50% or more of the organic carbon deposited typically escapes degradation

(Canfield et al. 2005). The GEM lagoon somehow deviates from this pattern, as it has a relatively high sedimentation rate ($> 0.1 \text{ g cm}^{-2} \text{ yr}^{-1}$), but the OC burial efficiency does not exceed 9%. The sediment of the GEM lagoon acts like an efficient reactor for OM mineralisation, which is possibly related to the high oxygen exposure of organic matter before and after deposition. The shallow depth (average = 0.8 m) of the lagoon enhances the wind-induced mixing, which counteracts stratification and oxygen depletion in summer. Combined with the deep oxygen penetration into the sediment (due to high pyrite burial – see below), this increases the oxygen exposure of the organic matter and hence could stimulate its overall degradation (Burdige 2007).

Organic carbon almost disappears below 30 cm (Fig. 3a), while sulphate is not completely consumed (Fig. 3c), which hence suggests that sulphate reduction is limited by organic matter availability. This is an uncommon observation in coastal environments, and one explanation for this could be the sedimentation history of the lagoon. Detailed interpretation of the radionuclide profiles by Flower et al. (2009) suggest that the sedimentation velocity has been relatively constant over the last 50 years, but that this was preceded in the late 1950s or early 1960s by an episode of very rapid sedimentation (with a sedimentation velocity that is four times higher than today). The sediment horizon at 28 cm was dated to the year 1960 (Flower et al. 2009), and so the low organic carbon values at depth (Fig. 3a) coincide with this high sedimentation interval. If primary production rates in the lagoon back then were equal or lower than today (e.g. due to less eutrophication), this would entail an overall dilution of the incoming organic matter, which hence could partially explain the low organic carbon values recorded below 30 centimetre. In deep sea environments, the organic matter flux to the sediment is generally low, and aerobic respiration is the principal pathway for the degradation of the organic matter in the sediment (Soetaert et al. 1996). When the water column is shallower, more organic matter arrives at the sediment surface, and so anoxic degradation pathways, including denitrification, iron reduction and sulphate reduction, become more important (Canfield et al. 1993). In coastal sediments, like lagoons and other transitional environments, more than 50% of organic matter is typically degraded by sulphate reduction (Lenzi 2010). This is also the case in the GEM lagoon, where sulphate reduction is estimated to account for 61 % of the mineralisation (Fig. 4a), and hence substantial production of free sulphide takes place within the sediment.

However, the relatively high input of iron oxides in the GEM lagoon prevents the build-up of free sulphide in the pore water. The biogeochemical model estimates that the contribution of dissimilatory iron reduction is small ($0.9 \text{ mmol m}^{-2} \text{ d}^{-1}$) and only accounts for 7% of the overall mineralisation (Fig. 4a). The simulated pore water profiles of both soluble and solid iron compounds agree well with the observed data, thus confirming that iron cycling is limited (Fig. 5). Sediment mixing is a crucial factor for iron reduction in marine sediments, as it ensures the continuous shuttling of iron between reduced and oxidised forms (Canfield 1994; Kristensen et al. 2000; Wijsman et al. 2002; van de Velde and Meysman 2016). Thamdrup et al. (1994) attributed the low contribution of dissimilatory iron reduction to the early diagenesis of OM in Aarhus Bay sediments to the low bioturbation rate. In contrast, iron reduction accounted for 84% to total OM mineralisation in Skagerrak sediments that are characterised by strong bioturbation (Canfield et al. 1993). As explained above, the sediment of the GEM lagoon does not show any signs of strong bioturbation activity, and in the model simulations, the bio-diffusion coefficient was set to a low value ($D_B = 0.1 \text{ cm}^2 \text{ yr}^{-1}$ over the first 10 cm). This low level of solid phase mixing in GEM lagoon thus explains the limited contribution of dissimilatory iron reduction. With higher levels of bioturbation (higher D_B), dissimilatory iron reduction becomes more important (up to 10% when $D_B = 6 \text{ cm}^2 \text{ yr}^{-1}$; van de Velde and Meysman, 2016).

3.2. Oxygen consumption

The simulated oxygen penetration depth of 13 mm is relatively large, while the total oxygen uptake (TOU) of the sediment as estimated by the model ($4.7 \text{ mmol m}^{-2} \text{ d}^{-1}$) is on the low end of estimates for coastal sediments. While this rate is almost double those reported by Svensson et al. (2000) in seagrass sediments of Venice lagoon, Italy ($2.4 \text{ mmol m}^{-2} \text{ d}^{-1}$) and by Alongi et al. (1996) in Ningaloo Reef lagoon ($2.8 \text{ mmol m}^{-2} \text{ d}^{-1}$), it is 2-4 times lower compared to those reported for other coastal lagoons (Eyre and Ferguson 2002, $12 \text{ mmol m}^{-2} \text{ d}^{-1}$ in seagrass sediments in 4 Australian lagoons; Dedieu et al. 2007, $8.4 \text{ mmol m}^{-2} \text{ d}^{-1}$ in the Thau lagoon; Rao et al. 2014, $6.8 \text{ mmol m}^{-2} \text{ d}^{-1}$ in a mesotidal lagoon in Netherlands). The GEM lagoon hence emerges as an environment characterised by intense and efficient organic matter processing (a relatively high mineralisation rate of $13.1 \text{ mmol C m}^{-2} \text{ d}^{-1}$ and a low burial efficiency of only 9%), but which requires little oxygen to accomplish this (a TOU of only $4.7 \text{ mmol m}^{-2} \text{ d}^{-1}$). As already noted above, this large discrepancy between TOU and mineralisation rate is a

direct consequence of the high burial flux of pyrite. Sulphide originating from sulphate reduction is trapped as pyrite and buried, and in this way, it is not re-oxidised back to sulphate. This lack of sulphide re-oxidation strongly reduces the sedimentary demand for oxygen, and also makes that the majority of the TOU (91%) is devoted to aerobic respiration.

As bio-irrigation is excluded from the model, and molecular diffusion is the only mode of transport for pore water solutes, the total oxygen uptake must be identical to the diffusive oxygen uptake of the sediment. The TOU was measured via darkened benthic chamber incubations in the GEM lagoon in 1990 and 2007 and TOU varies in the range of 9 and 21 mmol m⁻² d⁻¹ (Added 2002; Oueslati 2011). Accordingly, the predicted TOU is 2-4 times lower than the measured values. There are a number of factors that can explain this discrepancy. Firstly, the TOU predicted by the model reflects the long-term (~ years to decade) value of the TOU, as it is principally driven by the decomposition of low-reactive organic matter (generating O₂ demand) and burial flux of pyrite (decreasing O₂ demand). In contrast, TOU measurements by benthic chambers reflect short-time variations in TOU, and are, for example, dependent on season and the recent sedimentation history of organic matter. Additionally, the exclusion of nitrification from the model could contribute to the discrepancy. If the modelled TOU values are too low, then the actual O₂ penetration depth is underestimated, and in this case, a decreased O₂ exposure would lead to more organic carbon burial. The latter is nonetheless in contrast with the low burial efficiency observed. Still, with the presently available information, it is not possible to properly resolve the discrepancy between measured and modelled TOU. A more detailed study, in which TOU and DOU are measured concurrently, is required to better constrain the oxygen budget of the sediments in the GEM lagoon.

3.3 Nitrogen cycling

To match the observational data, the model needed to implement a very high C/N ratio= 50. Although coastal lagoons typically have higher C/N ratios than the Redfield ratio of 6.6 for marine phytoplankton, the GEM C/N ratio remains high compared to other lagoons, such as the Hog lagoon in Virginia (C/N = 10-19; Tyler et al. 2001), the Terminos lagoon in Mexico (C/N = 21-39; Rivera-Monroy et al. 1995), the New Caledonia lagoon (C/N = 6-30; Grenz et al. 2003). To test the sensitivity of the NH₄ depth profile towards the C/N ratio, we calculated steady state solutions with C/N values ranging from 7 to 50, keeping all other parameters constant (Fig. 6). The NH₄

depth profile varies strongly with the chosen C/N value, thus indicating that a high C/N ratio is needed to achieve a proper model fit. Ammonium adsorption onto the solid phase is not included in the model, but does not provide an explanation for the high C/N ratio. In steady-state simulations, as performed here, ammonium adsorption has no effect on the simulated depth profile of ammonium. Only in a transient state, adsorption will affect the simulated depth profile. It should be noted that the standard model includes a highly simplified N cycle (only ammonification is represented). As a sensitivity test, we extended the model with an active N-cycle (nitrification and denitrification). Overall, this only slightly modifies the simulated depth profiles (Fig 3). As expected, the gradient of the ammonium depth profile diminished near the sediment water interface: the efflux of ammonium out of the sediment was reduced, as all ammonium was now consumed by nitrification. Though beyond the first few centimeters, the explicit inclusion of nitrification and denitrification had very little effect on the depth profile of ammonium (Fig. 3f). Therefore, the inclusion of an active N-cycle cannot explain the need for a high C/N ratio.

A substantial part of the GEM lagoon is covered by seagrass, and a thick package of seagrass detritus (~50 cm thick) accumulates along the north-eastern shore, as a result of prevailing wind transport. Seagrass detritus is hence likely the main organic matter input in the GEM lagoon sediments. Seagrasses and macroalgae (seaweed) often have elevated C/N ratios because they contain higher levels of structural carbohydrates (lignin and cellulose) and lower amounts of protein (Prado and Heck 2011). Bianchi (2007) showed that the organic matter inputs of these vascular plants to coastal systems can cause problems for the interpretation of biogeochemical data because the C/N deviates markedly from the Redfield ratio. Seagrass detritus that is delivered from the shallower parts of the lagoon is the main organic matter input in the GEM lagoon sediments, and usually has a C/N ratio of around 25 for fresh material, and over 50 for aged material (Kristensen 1994; Duarte 1999). The increase with age is due to preferential nitrogen mineralisation during initial degradation. However, microbial biomass typically has a C/N ratio of 10 or less (Fenchel and Blackburn 1979), and so when aged seagrass detritus is degraded, the microbes need to acquire nitrogen from sources other than organic matter. Under these conditions, microbial growth will stimulate the uptake of NH_4^+ from the pore water (Kristensen et al. 2000). The GEM lagoon sediment is very rich in seagrass detritus (*Ruppia* sp.), which could explain the elevated C/N sediment ratio (50), while low ammonium values in the pore water could

be the result of efficient bacterial assimilation of dissolved inorganic nitrogen. In summary, the C/N ratio predicted by our model is substantially higher than commonly observed in coastal sediments. The hypothesis that sedimentary organic matter in the GEM lagoon has a high C/N ratio, and the cause of this, needs to be addressed in future studies, which should target direct measurements of the C/N ratio with $\delta^{13}\text{C}$ natural abundance of the sedimentary organic matter.

3.4. Iron and sulphur cycling and pyrite formation

Pyrite burial is a major sink of reduced sulphur and iron in the marine environment and is linked to the biogeochemical cycling of O, C, S, and Fe via bacterial sulphate reduction (Hurtgen et al. 1999). The degree of sulphurisation (DOS) and the degree of pyritisation (DOP) provide guidance on formation of iron sulphides and pyrite, and are calculated as:

$$DOS = \frac{(Fe-CRS)+(Fe-AVS)}{(Fe-CRS)+(Fe-reac)} \quad [3]$$

$$DOP = \frac{Fe-CRS}{(Fe-CRS)+(Fe-reac)} \quad [4]$$

where Fe-AVS is the Fe concentration calculated from AVS content (assuming that FeS is the major component) and Fe-CRS is the Fe concentration calculated from CRS content (assuming that FeS₂ is the major component). Fe-reac is the concentration of reactive iron in the sediment attacked by a cold HCl 1 M solution, and so this includes particulate carbonates, reactive iron oxides, and iron sulphide minerals (excluding pyrite). In the GEM lagoon sediment, AVS is a minor fraction by weight (<0.1 wt-% S), while CRS rapidly increases from 0.5 wt-% at the sediment-water interface to 1.2 wt-% at 23 cm depth (Fig. 7a). The DOS (0.26 to 0.63) and DOP (0.22 to 0.57) increase with the first 20 cm and remain thereafter constant with depth. (Fig. 7b), thus suggesting that the majority of the pyritisation takes place in the surface sediment, as has been noted for other coastal sediments (Brüchert 1998, Suits and Arthur 2000). The lower DOS and DOP values near the sediment-water interface are consistent with sediment deposition under fully oxygenated bottom-water conditions (Raiswell et al. 1988).

Surprisingly, even though sulphate reduction is responsible for the majority of the organic matter mineralisation (Fig. 4a; Oueslati et al. 2010), the pore water of the

lagoon is devoid of free sulphide (Added 2002). This suggests a tight coupling between sulphide production via sulphate reduction, and sulphide consumption by pyrite formation. Our simplified diagenetic model assumes that the HS⁻ production resulting from sulphate reduction becomes immediately available for FeS₂ formation. The model predicts a conversion efficiency from FeOOH to FeS₂ of > 0.89, which disagrees with the low values for DOS and DOP (Fig. 7b). Most likely, there is a considerable fraction of iron carbonates that contributes to Fe-reac fraction. Furthermore, the estimation of the Fe-reac fraction using the HCl extraction has been shown to extract iron from some silicate minerals that otherwise are considered unreactive (Kostka and Luther 1994), and thus DOS and DOP values might be underestimated.

However, both the low DOS and DOP values (Berner 1970; Dean and Arthur 1989; Raiswell and Berner 1985) as well as the model suggests that there is a surplus of reactive iron (0.27 mmol FeOOH m⁻² d⁻¹ is buried; Fig. 5). Consequently, the input of reactive iron oxides is not the limiting factor for pyrite formation. Another possible explanation for the low DOS and DOP values is a limited supply of sulphide, which can be either due to low sulphate availability or low organic matter availability (Berner 1984). Since sulphate is not depleted at depth (Fig. 3c), pyrite formation and burial in the GEM lagoon appears to be limited by the delivery of organic matter to the sediment surface.

3.5. Authigenic carbonate formation

Traditionally, marine sediments are considered places where carbonate dissolves, after its deposition from the water column. Still, authigenic carbonate precipitation has occasionally been observed in marine sediments (Reimers et al., 1996; Aller et al., 1996; Anderson and Dyrssen, 1987), and recently, Sun and Turchyn (2014) have proposed that the process might amount up to 10% of present-day global carbon burial. The sedimentary formation of authigenic carbonates is most relevant in coastal areas (Sun and Turchyn 2014).

Coastal sediments can thus either decrease or increase the inorganic carbon burial. Whether carbonates are formed or dissolved depends on the diagenetic processes in the sediment (Aller 2014). Shallow waters are generally supersaturated (Andersson et al. 2008), and so carbonate dissolution is restricted to the pore water. Oxygen has a pivotal role in the dissolution of carbonate, as the oxidation of reduced compounds like Fe²⁺

and FeS₂ consumes alkalinity (R4 and R5 in Table 5; Aller 2014), which promotes undersaturation with respect to carbonate phases like aragonite and calcite. In contrast, anaerobic mineralisation pathways (dissimilatory iron reduction, sulphate reduction) and pyrite precipitation increase the alkalinity of the pore water (Table 5), and will increase the saturation state. In the absence of dissolved Fe²⁺, however, the build-up of free sulphide during sulphate reduction can lead to the dissolution of carbonates at low sulphate reduction rates (Walter and Burton 1990).

Sedimentary carbonate increases and Ca²⁺ concentration decreases (Fig. 3i,j) due to the precipitation of authigenic carbonate. The model predicts a carbonate precipitation rate of 2.7 mmol m⁻² d⁻¹, which is an order of magnitude higher than the 0.2 mmol m⁻² d⁻¹ previously reported by Reimers et al. (1996) for muddy, unbioturbated sediments of the Santa Barbara Basin, and of a similar range as the 4 mmol m⁻² d⁻¹ found in coastal mudbanks of the Amazon delta (Aller et al. 1996; Zhu et al. 2002). Although the solid phase carbonate increase observed in the deeper sediment layers is explained in the model by Ca²⁺ consumption alone, it is possible that a small part of the authigenic carbonate formation could be linked to siderite (FeCO₃) precipitation (Jensen et al. 2002). Because the sediments of the GEM lagoon are carbonate rich by themselves (41%), the authigenic carbonate burial flux only accounts for ~5 % of the total inorganic carbon burial. One can expect that the importance of authigenic carbonates increases in sediments that receive less carbonate input from the overlying water.

Authigenic carbonate precipitation is stimulated by the generation of alkalinity during anaerobic mineralisation processes and pyrite formation (Table 5). Even though alkalinity is consumed during the precipitation of carbonate and the aerobic re-oxidation of Fe²⁺ and FeS₂, there is still a net production of alkalinity in the sediment of 3.4 mmol m⁻² d⁻¹, caused by high rates of alkalinity production by dissimilatory iron reduction and sulphate reduction (Table 5). This leads to an accumulation of alkalinity at depth (Fig. 3g), and generates an efflux of 3.4 mmol m⁻² d⁻¹, which is in the same range as the alkalinity fluxes estimated for estuarine bioturbated sediments (1.2 – 3.6 mmol m⁻² d⁻¹; Rao et al. 2014), sandy North-Sea sediments (1.7 – 6.6 mmol m⁻² d⁻¹; Brenner et al. 2016) or net alkalinity fluxes in Australian lagoon sediments colonised by seagrass (0 – 2 mmol m⁻² d⁻¹; Eyre and Ferguson 2002).

Overall, sedimentary alkalinity generation in coastal environments such as the GEM lagoon clearly play an important role in (i) the global carbon cycle via the precipitation, and subsequent burial, of authigenic carbonate and (ii) as a source of alkalinity to the

overlying water and open ocean, thus regulating ocean pH and CO₂ uptake (Thomas et al. 2009).

4. SUMMARY AND CONCLUSIONS

Diagenetic modelling showed that the sediment of the GEM Lagoon forms an efficient reactor for OM mineralisation, driven mainly by aerobic respiration in the upper layer of the sediment and sulphate reduction in deeper sediments. The ferrous iron (Fe²⁺) released from reduction of iron hydroxides (FeOOH) accumulates in the pore water, becoming thus available for pyrite formation (FeS₂). Pyritisation is fast in GEM Lagoon sediment, and is limited by organic matter availability. The anaerobic mineralisation pathways in organic matter mineralisation (sulphate reduction and dissimilatory iron reduction), produce a large amount of alkalinity that promotes authigenic carbonate precipitation. The sediments of the GEM lagoon hence are a significant source of alkalinity to the overlying water and likely positively contribute to the CO₂ buffer capacity of the coastal ocean.

5. ACKNOWLEDGEMENTS

The research leading to these results has received funding from the European Research Council through ERC Grants 306933 (FJRM). Furthermore, this research was financially supported by the Research Foundation Flanders (Odysseus grant G.0929.08 and FWO project grant G031416N to FJRM and an Aspirant PhD fellowship to SVDV) and the Netherlands Organisation for Scientific Research (VICI grant 016.VICI.170.072 to FJRM). SVDV is supported by a Fellowship of the Belgian American Educational Foundation.

6. REFERENCES

1. Added, A. 2001. Biogeochemical cycles of Org-C, Tot-N and Tot-S in the sediment of the Ghar El Melh Lagoon north of Tunisia. *J. Marine Syst.* 30 : 139-154.
2. Added, A. 2002. Cycles biogéochimiques des sels nutritifs, du fer, du manganèse et du soufre dans les sédiments de deux systèmes côtiers du nord de la Tunisie : Lagune de Ghar El Melh et lac Nord de Tunis. Doctoral thesis 266p, University of Tunis El Manar. Faculty of Sciences of Tunis.

3. Added, A. Ben Mammou, A. Abdeljaoued, S. Essonni, N. and Fernex F. 2003. Caractérisation géochimique des sédiments de surface du Golfe de Tunis. *Bull. Inst. Natn. Scien. Tech. Mer de Salammbô* 30 : 135-142.
4. Aller, R.C. 2014. Sedimentary Diagenesis, Depositional Environments, and Benthic Fluxes. *Treatise on Geochemistry* 2nd Edition, Elsevier, 293-334.
5. Aller, R.C. Blair, N.E. Xia, Q. and Rude, P.D. 1996. Remineralisation rates, recycling, and storage of carbon in Amazon shelf sediments. *Cont. Shelf Res.* 16: 753-786.
6. Alongi, D.M. Tirendi, F. and Goldrick, A. 1996. Organic matter oxidation and sediment chemistry in mixed terrigenous-carbonate sands of Ningaloo Reef, Western Australia. *Mar. Chem.* 54: 203-219.
7. Andersson, A.J. Mackenzie, F.T. and Bates, N.R. 2008. Life on the margin: implications of ocean acidification on Mg-calcite, high latitude and cold-water marine calcifiers. *Mar. Ecol. Prog. Ser.* 373: 265-274.
8. Ayache, F. Thompson, J.R. Flower, R.J. Boujarra, A. Rouatbi, F. and Makina, H. 2009. Environmental characteristics, landscape history and pressures on three coastal lagoons in the Southern Mediterranean Region: Merja Zerga (Morocco), Ghar El Melh (Tunisia) and Lake Manzala (Egypt). *Hydrobiologia*. doi:10.1007/s10750-008-9676-6.
9. Berg, P. Rysgaard, S. and Thamdrup, B. 2003. Dynamic modeling of early diagenesis and nutrient cycling: a case study in an Arctic marine sediment. *Am. J. Sci.* 303: 905-955.
10. Berner, A. 1970. Sedimentary pyrite formation. *Am. J. Sci.* 268: 1-23.
11. Berner R. A. 1974. Iron Sulfides in Pleistocene Deep Black Sea Sediments and Their Paleo-Oceanographic Significance: Geochemistry. In *The Black Sea--Geology, Chemistry, and Biology* (eds. E. T. Degens and D. A. Ross). American Association of Petroleum Geologists Memoir. 20:524–531
12. Berner, R.A. 1984. Sedimentary pyrite formation: An update. *Geochim.*

Cosmochim. Acta 48: 605–615.

13. Bianchi, T.S. 2007. *Biogeochemistry of Estuaries*. Oxford University Press, New York, NY, USA, 720 pp.

14. Boucher, G. Clavier, J. and Garrigue, C. 1994. Oxygen and carbon dioxide fluxes at the water-sediment interface of a tropical lagoon. *Mar. Ecol. Prog. Ser.* 107: 185-193.

15. Boudreau, B.P. 1996a. A method-of-lines code for carbon and nutrient diagenesis in aquatic sediments. *Comp. & Geosci.* 22: 479-496.

16. Boudreau, B.P. 1996b. The diffusive tortuosity of fine-grained unlithified sediments. *Geochim. Cosmochim. Acta* 60: 3139-3142.

17. Boudreau, B.P. 1997. *Diagenetic Models and Their Implementation*. Springer.

18. Brenner, H. Braeckman, U. Le Guitton, M. and Meysman, F.J.R. 2016. The impact of sedimentary alkalinity release on the water column CO₂ system in the North Sea. *Biogeosciences*. 13: 841-863.

19. Brown, P.N. Byrne, G.D. and Hindmarsh, A.C. 1989. VODE, a variable-coefficient ODE solver. *SIAM J Sci Stat Comput.* 10:1038-1051

20. Brüchert, V. 1998. Early diagenesis of sulfur in estuarine sediments: The role of sedimentary humic and fulvic acids. *Geochim. Cosmochim. Acta* 62: 1567-1586.

21. Burdige, D.J. 2007. Preservation of Organic Matter in Marine Sediments: Controls, Mechanisms, and an Imbalance in Sediment Organic Carbon Budgets?. *Chem. Rev.* 107: 467–485.

22. Canfield, D.E. 1994. Factors influencing organic carbon preservation in marine sediments. *Chem. Geol.* 114: 315-329.

23. Canfield, D.E. Jorgensen, B.B. Fossing, H. Glud, R. Gundersen, J. Ramsing,

- N.B. Thamdrup, B. Hansen, J.W. Nielsen, L.P. and Hall, P.O.J. 1993. Pathways of organic carbon oxidation in 3 continental margin sediments. *Mar. Geol.* 113: 27-40.
24. Canfield, D.E. Kristensen, E. and Thamdrup, B. 2005. Aquatic geomicrobiology. *Adv. Mar. Biol.* 48: 1-599.
25. Canfield, D.E. Raiswell, R. Westrich, J. Reaves, C. and Berner, R. 1986. The use of chromium reduction in the analysis of reduced inorganic sulfur in sediments and shales. *Chem. Geol.* 54: 149-155.
26. Clavero, V. Izquierdo, J.J. Fernandez, J.A. and Niell, F.X. 2000. Seasonal fluxes of phosphate and ammonium across the sediment-water interface in a shallow small estuary (Palmones River, southern Spain). *Mar. Ecol. Prog. Ser.* 198: 51-60.
27. Cyronak, T. Santos, I.R. Erler, D.V. and Eyre, B.D. 2013. Groundwater and porewater as major sources of alkalinity to a fringing coral reef lagoon (Muri Lagoon, Cook Islands). *Biogeosciences* 10: 2467-2480.
28. Dean, W.E. and Arthur, M.A. 1989. Iron-sulfur-carbon relationships in organic carbon rich sequences. I. Cretaceous western interior seaway. *Am. J. Sci.* 289: 708-743.
29. Dedieu, K. Rabouille, C. Thouzeau, G. Jean, F. Chauvaud, L. Clavier, J. Mesnage, V. and Ogier, S. 2007. Benthic O₂ distribution and dynamics in a Mediterranean lagoon (Thau, France): An in situ microelectrode study. *Est. Coast. Shelf Sci.* 72(3): 393-405.
30. Dhib, A. Ben Brahim, M. Ziadi, B. Akrouf, F. Turki, S. and Aleya, L. 2013. Factors driving the seasonal distribution of planktonic and epiphytic ciliates in a eutrophicated Mediterranean lagoon. *Mar. Pollut. Bull.* 76: 116-117.
31. Duarte, C. 1999. Seagrass ecology at the turn of the millennium: challenges for the new century. *Aquat. Bot.* 65: 7-20.
32. Eyre, B.D. and Ferguson, A.J.P. 2002. Comparison of carbon production and decomposition, benthic nutrient fluxes and denitrification in seagrass, phytoplankton,

benthic microalgae- and macroalgaedominated warm-temperate Australian lagoons. *Mar. Ecol. Prog. Ser.* 229: 43-59.

33. Faber, P. Kessler, A. Bull, J. McKelvie, I. Meysman, F. and Cook, P., 2012. The role of alkalinity generation in controlling the fluxes of CO₂ during exposure and inundation on tidal flats. *Biogeosciences* 9: 4087-4097.

34. Fenchel, T. and Blackburn, T.H. 1979. Bacteria and mineral cycling. Academic Press, New York.

35. Flower, R. J., et al. 2009. Sediment distribution and accumulation in lagoons of the Southern Mediterranean Region (the MELMARINA Project) with special reference to environmental change and aquatic ecosystems. *Hydrobiologia* 622(1): 85-112.

36. Froelich, P.N. Klinckhamer, G.P. Bender, M.L. Luedtke, N.A. Heath, G.R. Cullen, D. Dauphin, P. Hammond, D.E. Hartman, B. and Maynard, V. 1979. Early oxidation of organic matter in pelagic sediments of the eastern equatorial Atlantic: suboxic diagenesis. *Geochim. Cosmochim. Acta* 43: 1075-1090.

37. Gagnon, C. Mucci, A. and Pelletier, E. 1995. Anomalous accumulation of acid-volatile sulfides in a coastal marine sediment (Saguenay Fjord, Canada). *Geochim. Cosmochim. Acta* 59: 2663-2675.

38. Glud, R.N. 2008. Oxygen dynamics of marine sediments. *Mar. Biol. Res.* 4 : 243-289.

39. Grenz, C. Denis, L. Boucher, G. Chauvaud, L. Clavier, J. Fichez, R. and Pringault, O. 2003. Spatial variability in Sediment Oxygen Consumption under winter conditions in a lagoonal system in New Caledonia (South Pacific). *J. Exp. Mar. Biol. Ecol.* 285-286: 33-47.

40. Hofmann, A.F. Meysman, F.J.R. Soetaert, K. and Middelburg, J.J. 2008. A step-by-step procedure for pH model construction in aquatic systems. *Biogeosciences* 5,

227-251.

41. Hofmann, A.F. Soetaert, K. Middelburg, J.J. and Meysman, F.J.R. 2010. AquaEnv: An Aquatic Acid-Base Modelling Environment in R. *Aq. Geochem.* 16: 507-546.
42. Hu, X. and Cai W.-J. 2011. An assessment of ocean margin anaerobic processes on oceanic alkalinity budget. *Glob. Biogeochem. Cycles* 25, GB3003, <http://dx.doi.org/10.1029/2010GB003859>.
43. Huerta-Diaz, M.A. and Morse, J.W. 1990. A quantitative method for determination of trace metal concentrations in sedimentary pyrite. *Mar. Chem.* 29: 119-144.
44. Hull, V. Parrella, L. and Falcucci, M. 2008. Modelling dissolved oxygen dynamics in coastal lagoons. *Ecol. Model.* 211: 468-480.
45. Hurtgen, M.T. Lyons, T.W. Ingall, E.D. and Cruse, A.M. 1999. Anomalous enrichments of iron monosulfide in euxinic marine sediments and the role of H₂S in iron sulfide transformations: examples from Effingham Inlet, Orca Basin and the Black Sea. *Am. J. Sci.* 299: 556-588.
46. Jensen, Dorte, L. Boddum, J. K. Tjell, J.C. and Christensen, T.H. 2002. The solubility of rhodochrosite (MnCO₃) and siderite (FeCO₃) in anaerobic aquatic environments. *Appl. Geochem.* 4: 503-511.
47. Jourabchi, P. Van Cappellen, P. and Regnier, P. 2005. Quantitative interpretation of pH distributions in aquatic sediments: A reaction-transport modelling approach. *Am. J. Sci.* 305: 919-956.
48. Kostka, J.E. and Luther, III G.W. 1994. Partitioning and speciation of solid

phase iron in saltmarsh sediments. *Geochim. Cosmochim. Acta* 58: 1701-1710.

49. Kristensen, E. 1994. Decomposition of macroalgae, vascular plants and sediment detritus in seawater: Use of stepwise thermogravimetry. *Biogeochemistry* 26: 1-24.

50. Kristensen, E. Andersen, F.Ø. Holmboe, N. Holmer, M. and Thongtham, N. 2000. Carbon and nitrogen mineralisation in sediments of the Bangrong mangrove area, Phuket, Thailand. *Aquat. Microb. Ecol.* 22(2): 199-213.

51. Lenzi, M. 2010. Resuspension of sediment as a method for managing shallow eutrophic lagoons. *J. Ecol. Nat. Environ.* 2(11): 230-234.

52. Meysman, F.J.R. Boudreau, B.P. and Middelburg, J.J. 2005. Modeling reactive transport in sediments subject to bioturbation and compaction. *Geochim. Cosmochim. Acta* 69: 3601-3617.

53. Meysman, F.J.R. Middelburg, J.J. Herman, P.M.J. and Heip, C.H.R. 2003. Reactive transport in surface sediments. II. Media: an object-oriented problem-solving environment for early diagenesis. *Comp. & Geosci.* 29: 301-318.

54. Middelburg, J.J. Nieuwenhuize, J. Slim, F.J. Ohowa, B. 1996. Sediment biogeochemistry in an East African mangrove forest (Gazi Bay, Kenya). *Biogeochemistry* 34: 133-155.

55. Millero, F.J. Graham, T.B. Huang, F. Bustos-Serrano, H. and Pierrot, D. 2006. Dissociation constants of carbonic acid in seawater as a function of salinity and temperature. *Mar. Chem.* 100: 80-94.

56. Morse, J. Millero, F. Cornwell, J. and Rickard, D. 1987. The chemistry of the hydrogen sulfides and iron sulfides systems in natural waters. *Earth- Sci. Rev.* 24 : 1-42.

57. Moussa, M. Baccar, L. Ben and Khemis, R. 2005. La lagune de Ghar El Melh: Diagnostic écologique et perspectives d'aménagement hydraulique. *Rev. Sci. Eau* 18 :

13-26.

58. Nellemann, C. Corcoran, E. Duarte, C.M. Valdes, L. DeYoung, C. Fonseca, L. and Grimsditch, G. 2009. Blue Carbon. A Rapid Response Assessment. United Nations Environmental Programme, GRID-Arendal, Birkeland Trykkeri AS, Birkeland.

59. Nichols, M. Allen, G.P. 1981. Sedimentary process in coastal lagoons. In: Coastal Lagoon Research Present and Future. *UNESCO Technical papers in marine sciences* 33: 27-80.

60. Origel Moreno, M. 2015. Variabilité spatiale et temporelle des cycles biogéochimiques à l'interface eau-sédiment dans la lagune de Términos, Mexique. Thèse de doctorat, Institut Méditerranéen d'Océanologie, Université d'Aix-Marseille, Ecole Doctorale des Sciences de l'Environnement, 250 pp.

61. Oueslati, W. 2011. Cycles biogéochimiques des métaux lourds dans les sédiments marins de la lagune de Ghar El Melh. Doctoral thesis 274p, University of Tunis El Manar. Faculty of Sciences of Tunis.

62. Oueslati, W. Added, A. and Abdeljaoued, S. 2010. Geochemical and statistical approaches to evaluation of metal contamination in a changed sedimentary environment: Ghar El Melh Lagoon, Tunisia. *Chem. Speciat. Bioavailab.* 22 : 227-240.

63. Paskoff, R. 1981. L'évolution de la lagune littorale de Ghar el Melh. Delta de la Medjerda. Tunisie nord-orientale. *Bull. Soc. Langu. Géogr.* 15 : 49-57.

64. Paskoff, R. 1994. Le delta de la Medjerda (Tunisie) depuis l'antiquité. *Etudes Rurales* 133 : 15-29.

65. Pérez-Villalona, H. Cornwell, J.C. Ortiz-Zayas, J.R. and Cuevas, E. 2015. Sediment Denitrification and Nutrient Fluxes in the San José Lagoon, a Tropical Lagoon in the Highly Urbanized San Juan Bay Estuary, Puerto Rico. *Estuar. Coasts* 38 : 2259-2278.

66. Pimienta, J. 1959. Les cycles pliocènes–actuel dans les bassins paraliques de

Tunisie. Mémoires de la Soc. Géol. de France, nouvelle série 85, 176 p.

67. Prado, P. and Heck, Jr K.L. 2011. Seagrass selection by omnivorous and herbivorous consumers: determining factors. *Mar. Ecol. Prog. Ser.* 429: 45-55.
68. Raiswell, R. and Berner, R.A. 1985. Pyrite formation in euxinic and semi-euxinic sediments. *Am. J. Sci.* 285: 710-724.
69. Raiswell, R. Buckley, F. Berner, R.A. and Anderson, T.F. 1988. Degree of pyritization of iron as a paleoenvironmental indicator of bottom-water oxygenation. *J. Sediment. Petrol.* 58(5): 812-819.
70. Rao, A.M.F. Malkin, S.Y. Montserrat, F. and Meysman, F.J.R., 2014. Alkalinity production in intertidal sands intensified by lugworm bioirrigation. *Est. Coast. Shelf*

Sci. 148: 36-47.

71. Rao, A.M.F. Malkin, S.Y. Montserrat, F. and Meysman, F.J.R., 2016. Alkalinity production in intertidal sands intensified by lugworm bioirrigation. *Estuar. Coast. Shelf S.* 148: 36-47.

72. Rasmussen, E.K. Petersen, O.S. Thompson, J.R. Flower, R.J. Ayache, F. Kraiem, M. and Chouba, L. 2009. Model analyses of the future water quality of the eutrophicated Ghar El Melh lagoon (Northern Tunisia). *Hydrobiologia* 622: 173-193.

73. Rassmann, J. Lansard, B. Pozzato, L. and Rabouille, C. 2016. Carbonate chemistry in sediment porewaters of the Rhône River delta driven by early diagenesis (northwestern Mediterranean). *Biogeosciences* 13 : 5379-5394.

74. Regnier, P.A.G. Friedlingstein, P. Ciais, P. et al. 2013. Anthropogenic perturbation of the carbon fluxes from land to ocean. *Nat. Geosci.* 6: 597-607.

75. Reimers, C.E. Ruttenger, K.C. Canfield, D.E. Christiansen, M.B. and Martin, J.B. 1996. Porewater pH and authigenic phases formed in the uppermost sediments of the Santa Barbara Basin. *Geochim. Cosmochim. Acta.* 60: 4037-4057.

76. Rickard, D. 2006. The solubility of FeS. *Geochim. Cosmochim. Acta* 70, 5779-5789.

77. Rickard, D., Morse, J.W., 2005. Acid volatile sulfide (AVS). *Mar. Chem.* 97: 141-197.

78. Risgaard-Petersen, N. Revil, A. Meister, P. and Nielsen, L.P. 2012. Sulfur, iron, and calcium cycling associated with natural electric currents running through marine

sediment. *Geochim. Cosmochim. Acta* 92: 1-13.

79. Rivera-Monroy, V.H. Day, W.J. Twilley, R.R. Vera-Herrera, F. and Coronado-Molina, C. 1995. Flux of nitrogen and sediment in a fringe mangrove forest in Terminos Lagoon, Mexico. *Estuar. Coast. Shelf Sci.* 40: 139-160.

80. Rysgaard, S. Risgaard-Petersen, N. and Sloth, N.P. 1996. Nitrification, denitrification, and nitrate ammonification in sediments of two coastal lagoons in Southern France. *Hydrobiologia* 329: 133-141.

81. Sanchez-Cabeza, J.A. and Ruiz-Fernández, A.C. 2012. ²¹⁰Pb sediment radiochronology: An integrated formulation and classification of dating models. *Geochim. Cosmochim. Acta* 82: 183-200.

82. Schrag, D.P. Higgins, J.A. Macdonald, F.A. and Johnston, D.T., 2013. Authigenic Carbonate and the History of the Global Carbon Cycle. *Science* 339 : 540-543.

83. Shili, A. Trabelsi, E.B. and Ben Maïz, N. 2002. Benthic macrophyte communities in the Ghar El Melh lagoon (North Tunisia). *J. Coast. Conserv.* 8: 135-140.

84. Smith, P. Davis, S.J. Creutzig, F. et al. 2015. Biophysical and economic limits to negative CO₂ emissions. *Nat. Clim. Change*, doi:10.1038/NCLIMATE2870.

85. Soetaert, K. and Herman, P.M.J. 2009. A Practical Guide to Ecological Modelling. Using R as a Simulation Platform. Springer. ISBN 978-1-4020-8623-6.

86. Soetaert, K. and Meysman, F. 2012. Reactive transport in aquatic ecosystems: Rapid model prototyping in the open source software R. *Env. Mod. & Soft.* 32: 49-60.

87. Soetaert, K. Cash, J. and Mazzia, F. 2012. Solving Differential Equations in R, Springer. ISBN 978-3-642-28069-6, 248 pp.

88. Soetaert, K. Herman, P.M.J. Middelburg, J.J. 1996. A model of early diagenetic

processes from the shelf to abyssal depths. *Geochim. Cosmochim. Acta* 60: 1019-1040.

89. Soetaert, K. Petzoldt, T. and Setzer, R.W. 2010. Solving Differential Equations in R. *R Journal* 2: 5-15.

90. Stumm, W. and Morgan, J.J. 1996. Aquatic Chemistry: Chemical Equilibria and Rates in Natural Waters. Third Ed. John Wiley & Sons, New York, p. 1040.

91. Suits, N.S. and Arthur, M.A. 2000. Bacterial production of anomalously high dissolved sulphate concentrations in Peru slope sediments: steady-state sulfur oxidation, or transient response to end of El Nino?. *Deep-Sea Res. I* 47: 1829-1853.

92. Sun, X. and Turchyn, A.V. 2014. Significant contribution of authigenic carbonate to marine carbon burial. *Nature Geoscience* 7 : 20-204.

93. Svensson, J.M. Carrer, G.M. and Bocci, M. 2000. Nitrogen cycling in sediments of the Lagoon of Venice, Italy. *Mar. Ecol. Prog. Ser.* 199: 1-11.

94. Thamdrup, B. Fossing, H. and Jergensen, B.B. 1994. Manganese, iron and sulfur cycling in a coastal marine sediment. Aarhus Bay, Denmark. *Geochim. Cosmochim. Acta* 58: 5115-5129.

95. Thomas, H. Schiettecatte, L.S. Suykens, K. Koné, Y. Shadwick, E. Prowe, A. Bozec, Y. de Baar, H. and Borges, A. 2009. Enhanced ocean carbon storage from anaerobic alkalinity generation in coastal sediments. *Biogeosciences* 6: 267-274.

96. Tyler, A.C. McGlathery, K.J. and Anderson, I.C. 2001. Macroalgae Mediation of Dissolved Organic Nitrogen Fluxes in a Temperate Coastal Lagoon. *Est. Coast. Shelf Sci.* 53: 155-168.

97. Valdes, D.S. and Real, E. 2004. Nitrogen and phosphorus in water and sediments at Ria Lagartos coastal lagoon, Yucatan, Gulf of Mexico. *IJMS* 33(4): 338-345.

98. Van Cappellen, P. and Wang, Y.F. 1996. Cycling of iron and manganese in

surface sediments: A general theory for the coupled transport and reaction of carbon, oxygen, nitrogen, sulfur, iron, and manganese. *Am. J. Sci.* 296: 197-243.

99. van de Velde, S. and Meysman, F.J.R. 2016. The influence of bioturbation on iron and sulphur cycling in marine sediments: A model analysis. *Aquat. Geochem.* 22(5-6): 469-504.

100. Walter, L. M., and Burton, E.A. 1990. Dissolution of Recent platform carbonate sediments in marine pore fluids. *Am. J. Sci.* 290: 601-643.

101. Watanabe, K. and Kuwae, T. 2015. How organic carbon derived from multiple sources contributes to carbon sequestration processes in a shallow coastal system?. *Glob. Chang. Biol.* doi: 10.1111/gcb.12924.

102. Wijsman, J. Herman, P.M.J. Middelburg, J.J. and Soetaert, K. 2002. A Model for Early Diagenetic Processes in Sediments of the Continental Shelf of the Black Sea. *Est. Coast. Shelf Sci.* 54: 403-421.

103. Zaaboub, N. Martins, M.V.A. Dhib, A. Bejaoui, B. Galgani, F. El Bour, M. and Aleya, L. 2015. Accumulation of trace metals in sediments in a Mediterranean Lagoon: Usefulness of metal sediment fractionation and elutriate toxicity assessment. *Environ. Pollut.* 207: 226-237.

104. Zahar, Y. Ghorbel, A. and Albergel, J. 2008. Impacts of large dams on downstream flow conditions of rivers: Aggradation and reduction of the Medjerda channel capacity downstream of the Sidi Salem Dam (Tunisia). *J. Hydrol.* 351: 318-330.

105. Zhu, Z.B. Aller, R.C. and Mak, J. 2002. Stable carbon isotope cycling in mobile coastal muds of Amapa, Brazil. *Cont. Shelf Res.* 22: 2065-2079.



Figure 1. The Ghar El Melh (GEM) is a shallow coastal lagoon in northern part of Tunisia. The red marker denotes the location of the sampling site. The arrow indicates the narrow channel which allows water renewal through exchange with the Mediterranean.

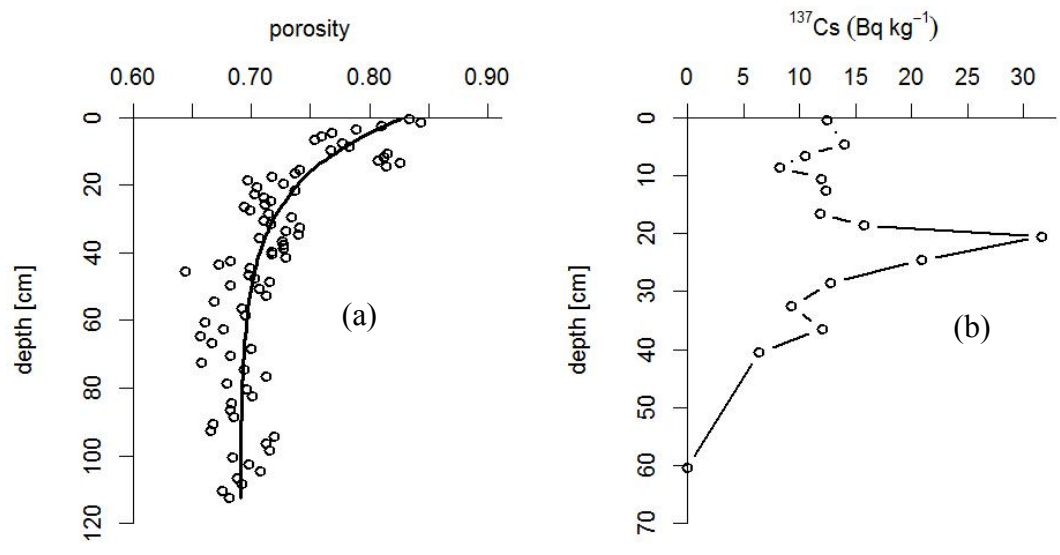


Figure 2. (a) Porosity depth profile. The solid line represents the exponential curve that was fitted through the data. (b) ^{137}Cs activity depth profile. Both profiles are reproduced from (Rasmussen et al., 2009).

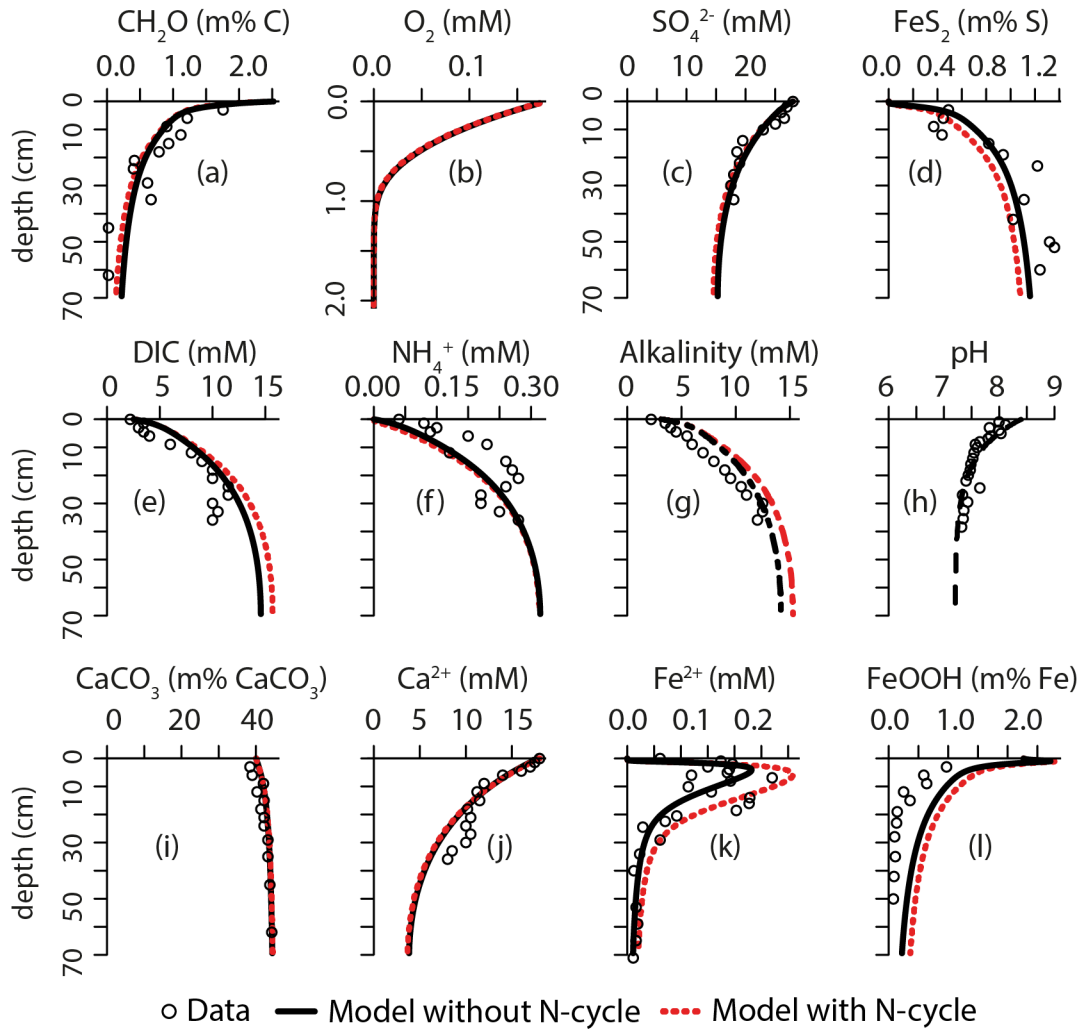


Figure 3. Concentration depth profiles of solutes and solids in the sediments from Ghar El Melh lagoon. Open markers indicate data, while continuous solid black lines and dotted red line represent model simulated profiles (black is model without an N-cycle, red model with an N-cycle). Dashed line for the pH indicates that pH was imposed and not calculated, and dashed-dotted line for alkalinity indicates that alkalinity was calculated from DIC and pH, and not explicitly modelled. Solute concentrations expressed in mM (alkalinity, NH_4^+ , O_2 , SO_4^{2-} , Fe^{2+} , Ca^{2+}), solid concentrations are expressed in expressed in mass % (organic matter, CaCO_3 , FeOOH and FeS_2). Note the different depth scale for the O_2 depth profile. Organic matter, pyrite, pH, CaCO_3 , dissolved iron and iron oxides were obtained from Oueslati (2011). Pore water sulphate, DIC, ammonium, alkalinity and dissolved calcium were obtained from Added (2001) and Added (2002).

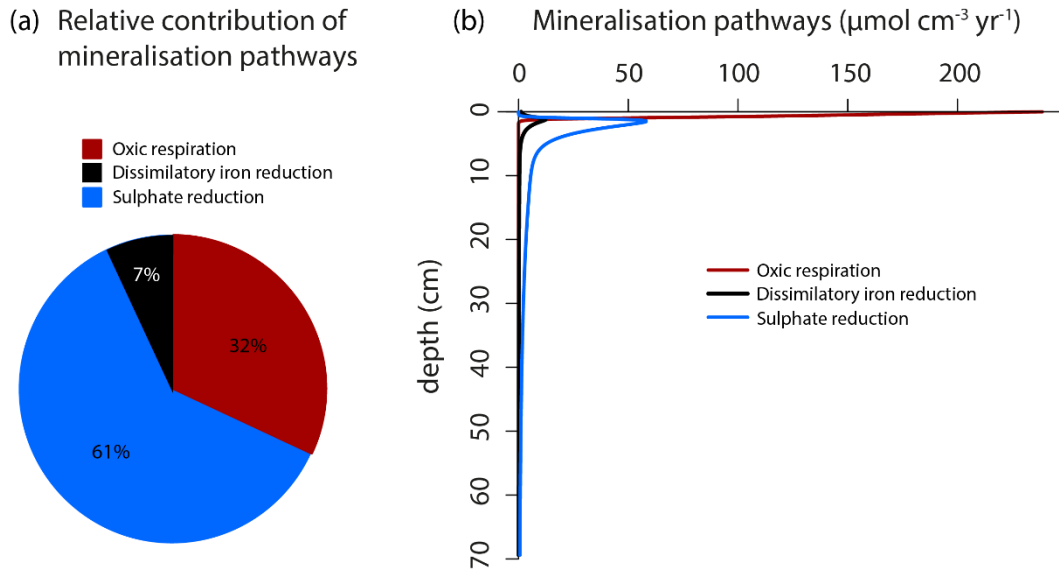


Figure 4. (a) Partitioning of the total organic matter mineralisation rate in different respiratory pathways. (b) Depth profiles of the rates of the different organic matter mineralisation pathways (same colour codes). Rates are taken from the model run without an N-cycle.

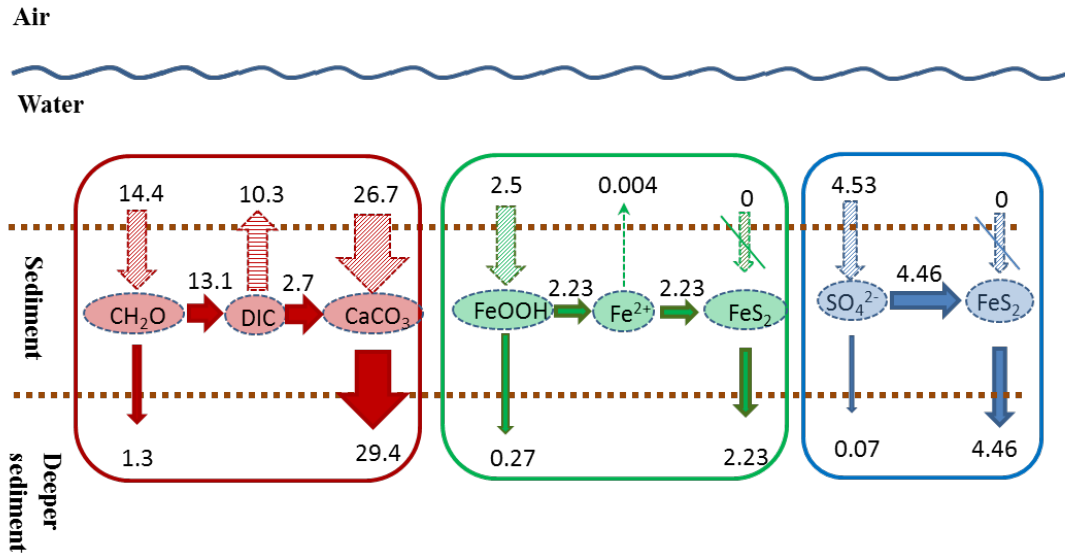


Figure 5. Steady state budget of carbon (red), iron (green) and sulphur (blue) in the sediments of the Ghar El Melh lagoon. Rates are expressed in $\text{mmol C / Fe / S m}^{-2} \text{ d}^{-1}$ respectively. Rates are taken from the model run without an N-cycle.

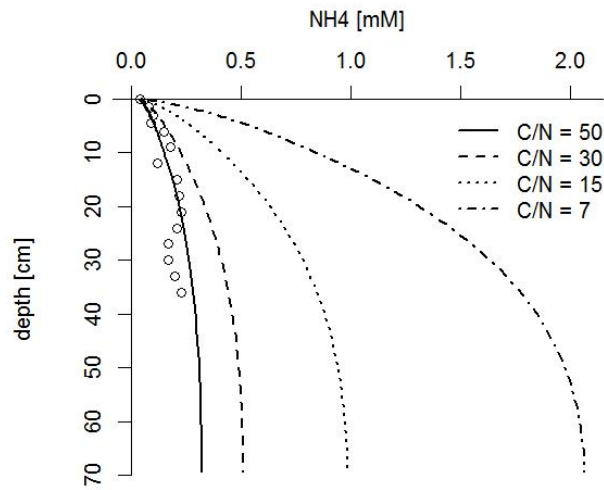


Figure 6. Sensitivity of steady-state ammonium depth profiles towards the C/N ratio of organic matter. The C/N value is varied from 7 (Redfield value) to 50. All other parameters are kept constant at the value tabulated in Table 1.

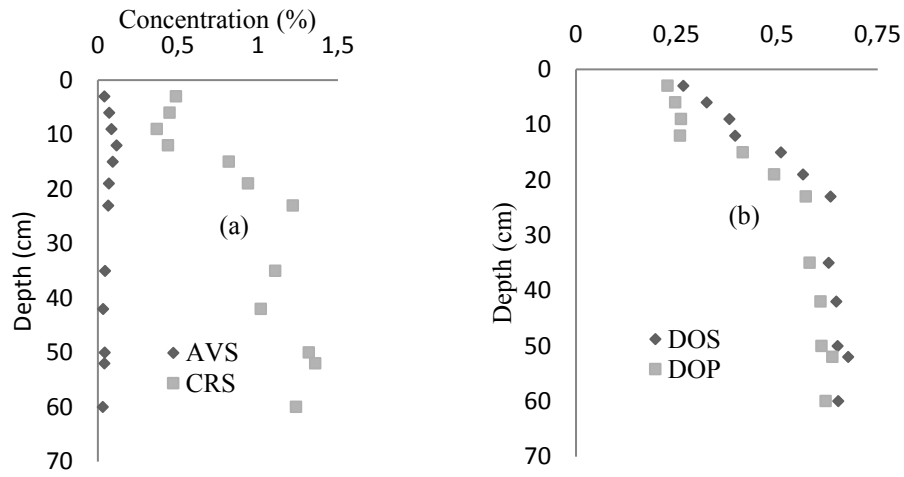


Figure 7. [a] Depth profiles of Acid Volatile Sulphide (AVS) and Chromium Reducible Sulphur (CRS) content. [b] Depth profiles of the Degree of Sulphurisation (DOS) and Degree of Pyritisation (DOP).

TABLES

ENVIRONMENTAL PARAMETERS	Symbol	Value	Units	Method	References
Temperature	T	30	°C	A	
Salinity	S	49	-	A	
Water depth	H	1.5	m	A	
Porosity (surface value)	ϕ_F^0	0.83	-	A	
Porosity (asymptotic at depth)	ϕ_F^∞	0.83	-	A	
Porosity attenuation coefficient	x_ϕ	19	cm	A	
Solid phase density	ρ_S	2.665	g cm ⁻³	A	
Sediment accumulation rate	F_{sed}	0.223	g cm ² yr ⁻¹	A	
Sedimentation velocity	v_0	0.50	cm yr ⁻¹	A	
Burial velocity	v_∞	0.27	cm yr ⁻¹	A	
Depth of sediment domain	L	72	cm	A	
BOUNDARY CONDITIONS	Symbol	Value	Units	Method	References
Oxygen bottom water	[O ₂]	0.2	mol m ⁻³	A	
Sulphate bottom water	[SO ₄ ²⁻]	28	mol m ⁻³	A	
DIC bottom water	∑CO ₂	2.2	mol m ⁻³	A	
Ammonium bottom water	[NH ₄ ⁺]	0.04	mol m ⁻³	A	
Calcium bottom water	[Ca ²⁺]	18	mol m ⁻³	A	
Ferrous iron bottom water	[Fe ²⁺]	0.06	mol m ⁻³	A	
Nitrate bottom water	[NO ₃ ⁻]	0.1	mol m ⁻³	A	
Flux OM fast decaying	F _{CH2O_F}	7.9	mmol m ⁻² d ⁻¹	F	
Flux OM slow decaying	F _{CH2O_S}	6.5	mmol m ⁻² d ⁻¹	F	
Flux FeOOH	F _{FeOOH}	2.5	mmol m ⁻² d ⁻¹	F	
Flux FeS ₂	F _{FeS2}	0	mmol m ⁻² d ⁻¹	F	
Flux CaCO ₃	F _{CaCO3}	27	mmol m ⁻² d ⁻¹	F	
BIOGEOCHEMICAL PARAMETERS	Symbol	Value	Units	Method	References
Mixing depth	L_{mix}	10	cm	A	
Biodiffusion coefficient	D_b	0.1	cm ² yr ⁻¹	A	
Mineralisation constant fast	k_f	0.5	yr ⁻¹	F	[1], [2]
Mineralisation constant slow	k_s	0.02	yr ⁻¹	F	[3], [4]
Oxygen saturation constant	K_{O_2}	0.008	mol m ⁻³	L	[3]
Nitrate saturation constant	$K_{NO_3^-}$	0.008	mol m ⁻³	L	[3]
FeOOH saturation constant	K_{FeOOH}	1.88	mmol g ⁻¹	L	[3]
Sulphate saturation constant	$K_{SO_4^{2-}}$	0.9	mol m ⁻³	L	[3]
C/N ratio organic matter	β	50	-	F	
NH ₄ ⁺ oxidation rate constant	k_{AMO}	10 ⁺⁵	mol ⁻¹ m ⁻³ yr ⁻¹	L	[3]
Fe ²⁺ oxidation rate constant	k_{FIO}	10 ⁺⁶	mol ⁻¹ m ³ yr ⁻¹	L	[3]
FeS ₂ oxidation rate constant	k_{PO}	10 ⁺²	mol ⁻¹ m ³ yr ⁻¹	L	[3]
CaCO ₃ precipitation rate constant	k_{CP}	1.5	mol m ⁻³ yr ⁻¹	L	[3]

CaCO ₃ precipitation exponent	n_{CP}	1	-	L	[3]
--	----------	---	---	---	-----

Table 1. List of parameters included in the model. The sedimentation velocity is calculated as $v_0 = F_{sed} / (\rho_s (1 - \phi_F^0))$, while the burial velocity is calculated as $v_\infty = F_{sed} / (\rho_s (1 - \phi_F^\infty))$. “Method” refers to the procedure by which parameter values are constrained: A = Measurements, L = Literature values, F = fitted. References: [1] Soetaert et al., (1996) [2] Boudreau (1997) [3] Meysman et al. (2003) [4] Van Cappellen and Wang (1996).

Kinetic reactions		
R1	Aerobic respiration	$(CH_2O)(NH_3)_{1/\beta} + O_2 \rightarrow HCO_3^- + \frac{1}{\beta} NH_4^+ + \frac{\beta-1}{\beta} H^+$
R*	Denitrification	$(CH_2O)(NH_3)_{1/\beta} + \frac{4}{5} NO_3^- + \frac{4\beta+5}{5\beta} H^+ \rightarrow \frac{2}{5} N_2 + HCO_3^- + \frac{1}{\beta} NH_4^+ + \frac{2}{5} H_2O$
R2	Dissimilatory Iron reduction	$(CH_2O)(NH_3)_{1/\beta} + 4FeOOH + \frac{7\beta+1}{\beta} H^+ \rightarrow HCO_3^- + \frac{1}{\beta} NH_4^+ + 4Fe^{2+} + 6H_2O$
R3	Sulphate reduction	$(CH_2O)(NH_3)_{1/\beta} + \frac{4}{7} SO_4^{2-} + \frac{2}{7} Fe^{2+} \rightarrow HCO_3^- + \frac{1}{\beta} NH_4^+ + \frac{2}{7} FeS_2 + \frac{3\beta-7}{7\beta} H^+ + \frac{2}{7} H_2O$
R**	Ammonium oxidation	$NH_4^+ + 2O_2 \rightarrow NO_3^- + H_2O + 2H^+$
R4	Ferrous iron oxidation	$Fe^{2+} + \frac{1}{4} O_2 + \frac{3}{2} H_2O \rightarrow FeOOH + 2H^+$
R5	Pyrite oxidation	$FeS_2 + \frac{7}{2} O_2 + H_2O \rightarrow Fe^{2+} + 2SO_4^{2-} + 2H^+$
R6	Carbonate precipitation	$Ca^{2+} + HCO_3^- \rightarrow CaCO_3 + H^+$

Table 2. List of biogeochemical reactions included in the sediment model. Organic matter is described as a amino-carbohydrate, having β carbons for 1 nitrogen. Note that the model includes fast and slow reacting organic matter fractions, that are implemented with different kinetic constants. R* and R**: denitrification and ammonium oxidation are not included in the standard model, only as a sensitivity test (see Fig. 3).

Reaction	Kinetic rate expression
Mineralisation	$R_{\min,s} = (1 - \phi_F) k_s [(CH_2O) \cdot (NH_3)_{1/\beta}]$ $R_{\min,f} = (1 - \phi_F) k_f [(CH_2O) \cdot (NH_3)_{1/\beta}]$
R1 Aerobic respiration	$R = R_{\min,f} \frac{[O_2]}{[O_2] + K_{O_2}}$
R* Denitrification	$R = R_{\min,f} \frac{K_{O_2}}{[O_2] + K_{O_2}} \frac{[NO_3^-]}{[NO_3^-] + K_{NO_3^-}}$
R2 Iron reduction	$R = R_{\min,f} \frac{K_{O_2}}{[O_2] + K_{O_2}} \frac{K_{NO_3^-}}{[NO_3^-] + K_{NO_3^-}} \frac{[FeOOH]}{[FeOOH] + K_{FeOOH}}$
R3 Sulphate reduction	$R = R_{\min,f} \frac{K_{O_2}}{[O_2] + K_{O_2}} \frac{K_{NO_3^-}}{[NO_3^-] + K_{NO_3^-}} \frac{K_{FeOOH}}{[FeOOH] + K_{FeOOH}} \frac{[SO_4^{2-}]}{[SO_4^{2-}] + K_{SO_4^{2-}}} \frac{[Fe^{2+}]}{[Fe^{2+}] + K_{Fe^{2+}}}$
R** Ammonium oxidation	$R = \phi_F k_{AMO} [NH_4^+] [O_2]$
R4 Ferrous iron oxidation	$R = \phi_F k_{FIO} [Fe^{2+}] [O_2]$
R5 Pyrite oxidation	$R = (1 - \phi_F) k_{PO} [O_2] [FeS_2]$
R6 Carbonate precipitation	$R = (1 - \phi_F) k_{CP} \left(\frac{[Ca^{2+}][CO_3^{2-}]}{K_{CaCO_3}^{SP}} - 1 \right)^{n_{CP}}$

Table 3. List of kinetic rate expressions for the reactions included in the model. The model includes fast and slow reacting organic matter fractions, that are implemented with different kinetic constants. Note that reactions R1, R2 and R3 are only shown for the fast reacting fraction. The slow reacting fractions is implemented identically. R* and R**: denitrification and ammonium oxidation are not included in the standard model, only as a sensitivity test (see Fig. 3).

MINERALISATION RATE	STUDY SITE	REFERENCE
13.1	Ghar El Melh lagoon, Tunisia	This study
7.2 - 8.2	Thau lagoon, France	Dedieu et al. (2007)
21	Fogliano lagoon, Italy	Hull et al. (2008)
29 – 48	Términos lagoon, Mexico	Origel Moreno (2015)
44 – 61	Gazi lagoon, Kenya	Middelburg et al. (1996)
60	New Caledonia lagoon, France	Boucher et al. (1994)
46 - 102	Australian lagoons	Eyre and Ferguson (2002)

Table 4. Mineralisation rate of organic matter ($\text{mmol C m}^{-2} \text{d}^{-1}$) in the GEM lagoon sediment as compared to other coastal lagoons and embayments.

		REACTION	$\Delta A_T / \Delta DIC$	RATE
R1	Aerobic mineralisation	$(CH_2O)(NH_3)_{1/\beta} + O_2 \rightarrow HCO_3^- + \frac{1}{\beta} NH_4^+ + \frac{\beta-1}{\beta} H^+$	0 / +1	4.26
R2	Iron reduction	$(CH_2O)(NH_3)_{1/\beta} + 4FeOOH + \frac{7\beta+1}{\beta} H^+ \rightarrow$ $HCO_3^- + \frac{1}{\beta} NH_4^+ + 4Fe^{2+} + 6H_2O$	+8 / +1	0.9
R3	Sulphate reduction with pyrite precipitation	$(CH_2O)(NH_3)_{1/\beta} + \frac{4}{7} SO_4^{2-} + \frac{2}{7} Fe^{2+} \rightarrow$ $HCO_3^- + \frac{1}{\beta} NH_4^+ + \frac{2}{7} FeS_2 + \frac{3\beta-7}{7\beta} H^+ + \frac{2}{7} H_2O$	+0.57 / +1	7.9
R4	Iron oxidation	$Fe^{2+} + \frac{1}{4} O_2 + \frac{3}{2} H_2O \rightarrow FeOOH + 2H^+$	-2 / 0	1.4
R5	Pyrite oxidation	$FeS_2 + \frac{7}{2} O_2 + H_2O \rightarrow Fe^{2+} + 2SO_4^{2-} + 2H^+$	-2 / 0	0.04
R6	Carbonate precipitation	$Ca^{2+} + HCO_3^- \rightarrow CaCO_3 + H^+$	-2 / -1	2.7

Table 5: Reaction rates (integrated with depth and expressed in $\text{mmol m}^{-2} \text{d}^{-1}$) for all reactions in the reaction list. The change in alkalinity (ΔA_T) and dissolved inorganic carbon (ΔDIC) due to each reaction is also listed.